TECHNICAL REPORT R-77

FLOW IN THE BASE REGION OF AXISYMMETRIC AND TWO-DIMENSIONAL CONFIGURATIONS

By MILTON A. BEHEIM

Lewis Research Center
Cleveland, Ohio

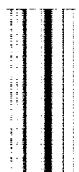

TECHNICAL REPORT R–77

FLOW IN THE BASE REGION OF AXISYMMETRIC AND TWO-DIMENSIONAL CONFIGURATIONS

By Milton A. Beheim

SUMMARY

A theoretical and experimental investigation has been conducted of the pressure distribution on the surface of either a circular cylinder or a truncated cone located within the base region of another circular cylinder at Mach number 2. A similar analysis of pressure distribution was made for rearward-facing two-dimensional steps, and theoretical results were compared with experimental results of earlier investigations. Theoretical base-pressure ratios of two-dimensional steps agreed well with experimental results; however, as a result of the simplifying assumptions made for axisymmetric configurations, only a range of values for theoretical base-pressure ratio could be calculated within which the experimental results were expected to occur. The data generally followed the trends predicted by the theory, and deviations apparently could be explained.

The location of the start of the pressure rise on the surface downstream of either a two- or three-dimensional step and the magnitude of the pressure rise could be predicted fairly well with the theory. The shape of the predicted pressure-rise curve agreed more closely with experiment for the smaller step sizes. In all cases the distance required to complete the pressure rise was greater than theory. The effects of base bleed on base-pressure ratio of axisymmetric configurations were also calculated and agreed well with experimental results at low bleed flow rates.

INTRODUCTION

Details of the flow in the base region of two-dimensional and axisymmetric backward-facing steps are of interest but have proved difficult to determine analytically. The need for a satisfactory method of analyzing this type of flow (in particular to determine its pressure distribution) is evident in current studies of the flow in the base region of a missile (to determine gimbal moments, drag, heating, etc.) and of the flow between stages of a missile as the stages separate. General analyses that have contributed much to an understanding of this flow problem are those such as references 1 and 2. Both studies were concerned chiefly with two-dimensional flows. In reference 1 the theoretical calculation of base pressure of a two-dimensional step agreed well with experiment. In reference 3, Chapman presented some analysis of the base flow for axisymmetric bodies but did not develop the analysis to the extent that base pressure could be calculated.

The present study combines and extends the analyses of references 1 to 3 in an attempt to calculate the base pressure of an axisymmetric configuration and the pressure distribution on the surface downstream of either a two-dimensional or an axisymmetric step. Effects of base bleed with axisymmetric configurations were also studied. Experimental data obtained in the Lewis 8- by 6-foot supersonic tunnel with axisymmetric configurations were used as a guide in the analysis and also were used to determine the accuracy of the theoretical calculations. Earlier published data were used to verify the two-dimensional calculations.

ANALYTICAL FLOW MODEL

A flow model for use in theoretical analysis of two-dimensional flow over a backward-facing step has been described in references 1 and 2, and a corresponding model for axisymmetric flow has been partially described in reference 3. The model for axisymmetric flow used in the present analysis was based on these earlier models and is illustrated in figure 1.

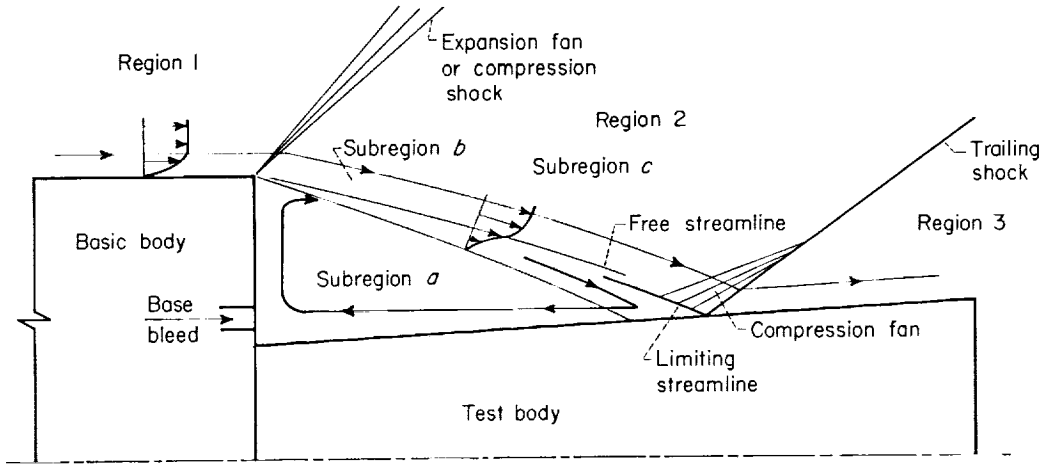

FIGURE 1. Flow model.

Three main regions are considered. Upstream of the base (region 1) the flow is determined by the body shape and the free-stream Mach number, and details can be obtained from characteristic solutions and the boundary-layer equations. In region 2, between the waves emanating from the step edge and those associated with the trailing shock, the flow is governed by the pressure in the dead-air region (subregion *a*). In the mixing zone (subregion *b*), velocities are governed by whether the mixing is turbulent or laminar and by the size and shape of the initial boundary layer (see refs. 4 and 5).

From continuity considerations, all flow from region 1 plus any bleed flow must pass downstream through the trailing shock. There will exist, then, within subregion *b* a streamline, the limiting streamline, which divides the flow that ultimately passes downstream from that which recirculates. The mass flux between the limiting streamline and the innermost streamline of the flow from region 1, the free streamline, is equal to the base-bleed flow rate. The maximum pressure rise that can be sustained by the flow along the limiting streamline determines the possible strength of the trailing shock and hence is a factor in determining base pressure.

In subregion *c* of region 2 the flow can be determined by a characteristic solution. In region 3, downstream of the trailing shock, conditions are determined by the shape of the test body and by conditions in region 2. The nature of the flow at the base of the trailing shock is of importance, since the pressure rise in this region is the second factor that determines base pressure (i.e., base pressure is equal to region 3 pressure divided by the allowable pressure rise of the limiting streamline), and it also determines the local pressure distribution.

Several complications arise that make the preceding calculations very difficult. One such complication occurs in determining the flow in subregion *c* for a given base-pressure ratio. For axisymmetric configurations a characteristic net must be determined for the entire region, since the streamlines are curved. In addition, the waves that emanate from the step edge interact with the boundary layer, producing secondary waves in subregion *c* (see ref. 6) for either two- or three-dimensional configurations. Characteristic solutions of these types are fairly long and tedious.

The velocity profile across the mixing region upstream of the trailing shock is also difficult to obtain; yet it is needed to determine the allowable pressure rise of the limiting streamline. This profile is affected by the following: the properties of the initial boundary layer, the waves emanating from the step edge, the distance through the mixing zone from the step edge to the point in question, the nature of the mixing process (laminar or turbulent), and local effects of shear near the trailing shock caused by the reversed flow and the test-body surface.

Another complication is encountered in determining the trailing-shock pressure rise and the shape of the rise curve. Near the test body a compression fan exists. In order to determine the structure of this fan, and hence the pressure-

rise curve, it would be necessary to know the details of the approaching flow in subregions *b* and *c* plus details of the reversed flow and their interactions. Such a calculation would be very difficult. At some distance from the test body the waves of this fan would coalesce into a single shock wave. With two-dimensional configurations, this wave would also be two-dimensional; however, with axisymmetric configurations an additional complication arises in that the strength of this shock would vary with distance from the test body because of the three-dimensionality of the flow. Close to the test-body surface it would be approximately two-dimensional in character, and at sufficiently large distances it would be nearly conical. Thus, an additional characteristic solution would be required.

Obviously, many simplifications are needed to make the problem amenable to solution. Those used in the present study are as follows:

(1) The flow in region 1 was uniform, and the presence of an initial boundary layer was neglected. This assumption is needed to simplify steps (2) and (3) below.

(2) For axisymmetric configurations the nonmixing flow properties in subregion *c* of the free streamline were determined from the characteristic solutions of reference 7, assuming the presence of the test body had no effect on these properties upstream of the intersection of the free streamline and the test body. It was further assumed that flow direction along all other streamlines in subregion *c* just ahead of the trailing shock was uniformly equal to that for the free streamline. For two-dimensional steps a simple Prandtl-Meyer expansion to base pressure was used, and all streamlines in subregion *c* were straight and parallel.

(3) The velocity profile of the mixing zone was fully developed ahead of the trailing shock, and the mixing process was either turbulent or laminar. The results of reference 8 for turbulent mixing and of reference 5 for laminar mixing, which were derived for two-dimensional flow, were used without correction for three-dimensional effects. All effects of the reversed flow and the test-body surface on the velocity profile ahead of the trailing shock were neglected. This mixing profile was superimposed upon the characteristic flow discussed earlier so that the jet boundary streamline (in the nomenclature of ref. 1) coincided with the free streamline.

(4) Each streamline inside the limiting streamline stagnated isentropically at the test-body surface before flowing back upstream; those outside the limiting streamline passed downstream through the trailing shock. This process was assumed to occur along each streamline without effect on adjacent streamlines. The resulting pressure rise was thus dependent on the shape of the velocity profile and its orientation with respect to the test-body surface.

(5) The presence of a compression fan was neglected, and the trailing shock was a single wave originating from the intersection of the test-body surface and the limiting streamline. For two-dimensional configurations this wave was also two-dimensional and turned the flow parallel to the surface downstream of the step. For axisymmetric configurations two calculations were made. In one it was assumed that the trailing shock was a plane wave that turned the flow parallel to the test-body surface. In the other it was assumed that it was a conical wave produced by a hypothetical cone with a half-angle equal to the difference in approaching flow direction and test-body surface direction. These waves were assumed because the actual trailing-shock strength is probably somewhere between these two assumptions, and because these shock-wave properties are well-known and widely tabulated.

Theoretical calculations to determine the effect of base bleed were based on the analysis of reference 1 but are here applied to axisymmetric flows. The essential feature that distinguishes base-bleed calculations from the no-bleed case is that the limiting streamline no longer coincides with the free streamline. As in reference 1 it was assumed that the axial momentum of the bleed flow was negligible.

EXPERIMENTAL APPARATUS AND PROCEDURE

The experimental data for the axisymmetric configurations of the present study were obtained in the Lewis 8- by 6-foot supersonic tunnel at a free-stream Mach number of 1.98. The schematic sketch of figure 2(a) shows the installation in the tunnel. Two struts supported the cone-cylinder combination, which will be referred to as the basic body; and located in its base region were a variety

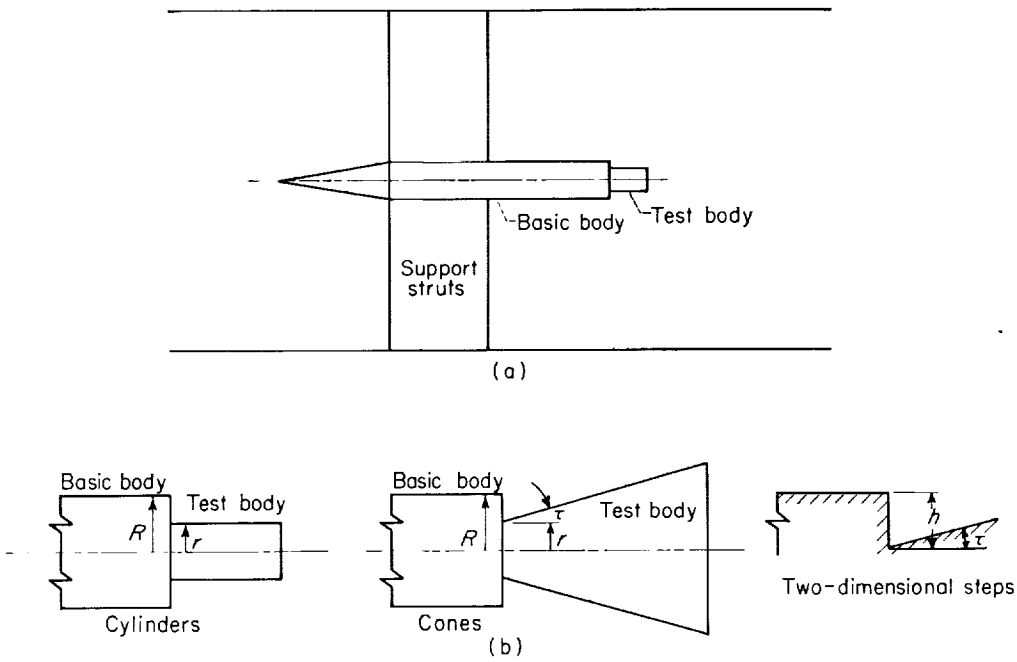

(a) Schematic sketch of tunnel installation.
(b) Test-body geometry.
FIGURE 2.—Model geometry.

TABLE I.—AXISYMMETRIC CONFIGURATIONS
[M_0, 1.98; boundary-layer-thickness ratio, δ/d, 0.125.]

Radius ratio, r/R	Cone half-angle, τ, deg
Cylinders	
0.875	--------
.75	--------
.5	--------
.25	--------
Cones	
0.475	15
.31	15
.125	15
.715	25
.425	25
.122	25

of cylinders and truncated cones referred to as test bodies. Although these configurations were used in a general study of base flow, the models were representative of geometries that can be encountered in missile designs where the rocket motor extends downstream of the base, and also encountered as missile stages separate. Sketches of the test bodies appear in figure 2(b) as an aid in defining symbols for geometric parameters, and a list of the values of these parameters is presented in table I. A list of symbols and their definitions appears in appendix A. Four cylinder sizes and two cone angles were selected. The cones (which were mounted to the basic body by means of a screw jack) were translated with respect to the base of the basic body so as to vary the radius ratio r/R. In all cases the base region between the basic body and the test body was open to the interior of the basic body.

The test bodies were instrumented with a row of static-pressure orifices along one or two elements to determine the pressure distribution in the region of the trailing shock. Static-pressure orifices located in the interior of the basic body just upstream of the plane of the base were used to determine base pressure. With each test body, data were obtained over a range of base bleed flows. Air for base bleed was supplied from a source external to the tunnel and ducted into the model

TABLE II.—TWO-DIMENSIONAL CONFIGURATIONS

Test Mach number, M_0	Step angle, τ, deg	Boundary-layer-thickness ratio, δ/h	Reference
1.7	0	----------	2
2.0	0	----------	2
2.3	0	0.125	15
2.48	0	.100	16
1.86	7	.23	16
1.86	12	.23	16
1.86	16½	.23	16

through the support struts. Orifice plates were used to determine this flow rate.

Experimental data from other literature for two-dimensional steps were also used in the present analysis. A sketch of this type of configuration is also shown in figure 2(b) to define symbols, and a list of the model geometrical parameters and the appropriate references appears in table II.

RESULTS AND ANALYSIS

TWO-DIMENSIONAL CONFIGURATIONS

For two-dimensional configurations, step height is of significance only in that its size relative to initial boundary-layer thickness is a factor in determining whether sufficient distance exists between the step edge and the trailing shock to permit fully developed mixing. The boundary-layer-thickness ratio for the data used in the present study is tabulated in table II.

Experimental and theoretical base-pressure ratios for several two-dimensional-step configurations are presented in figure 3. Figure 3(a) shows the effect of approach Mach number on the base-pressure ratio with zero step angle. ("Step angle" refers to the angularity of the surface downstream of the step as illustrated in figure 2(b).) Theoretical calculations based on the analyses of references 1 and 2 were made for both laminar and turbulent mixing, and details are described in appendix B. At Mach 2.0 the experimental base-pressure ratio with turbulent mixing

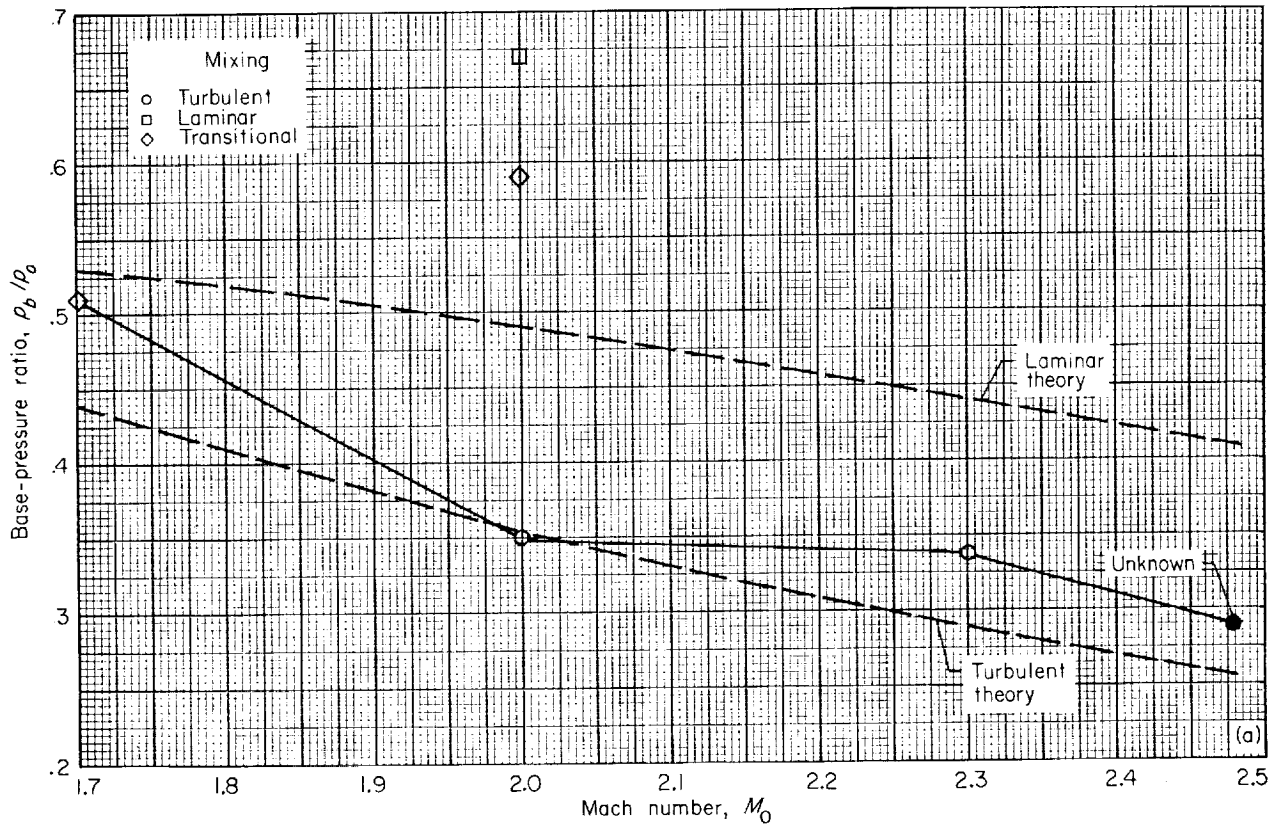

(a) Effect of Mach Number. Step angle, τ, 0°.

FIGURE 3.—Base-pressure ratio of two-dimensional steps.

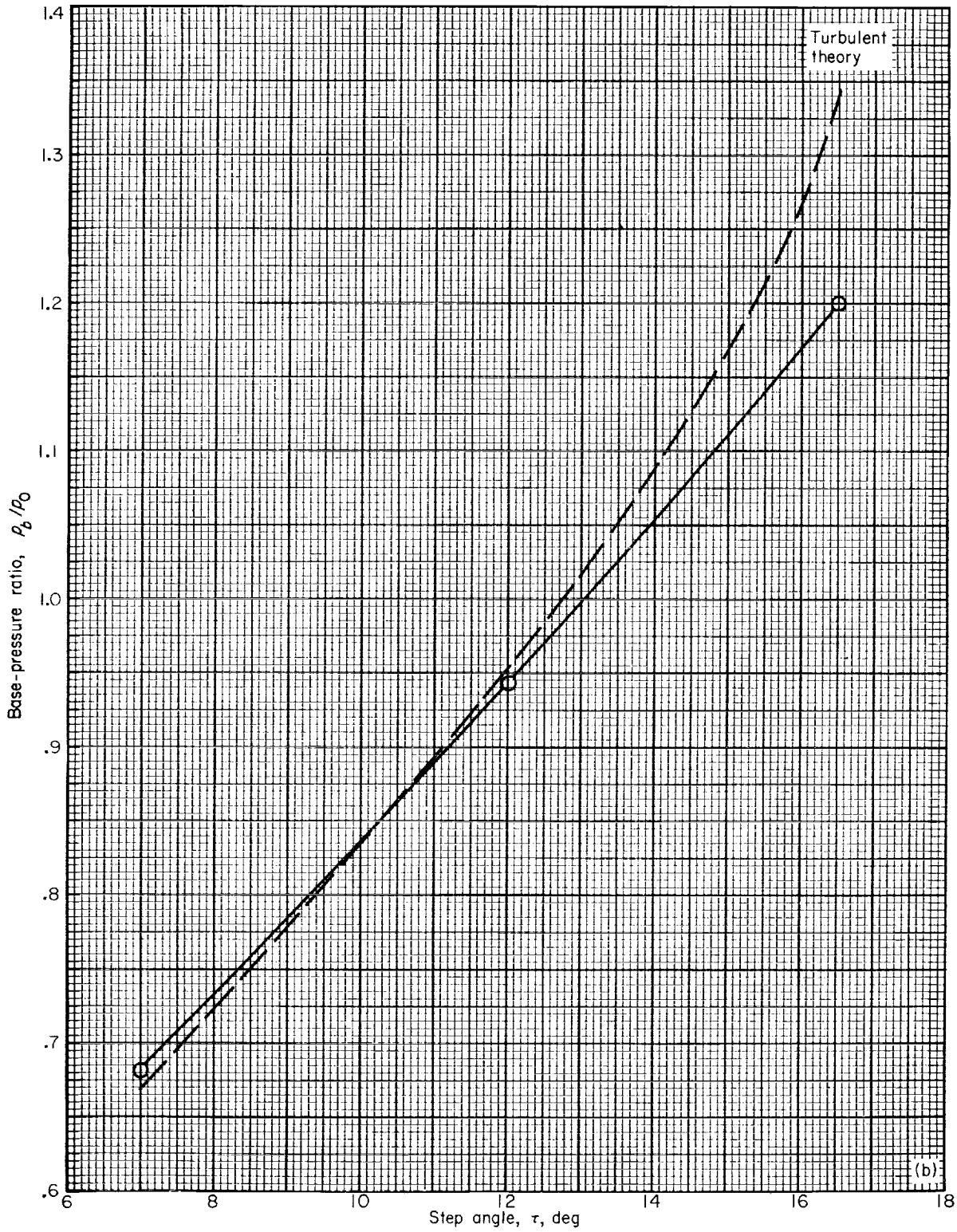

(b) Effect of step angle. Mach number, 1.86.

FIGURE 3.– Concluded. Base-pressure ratio of two-dimensional steps.

was in excellent agreement with turbulent theory, but with laminar mixing the ratio was higher than laminar theory. With an initial boundary layer it is known that the distance from the beginning of mixing to the point where a fully developed profile is achieved is greater for laminar than for turbulent mixing. Reference 1 has shown that the effect of a profile that is not fully developed is to increase the base pressure. In addition, reference 2 has shown that with negligible initial boundary layer the laminar theory and data are in good agreement. Therefore, it appears that the discrepancy between laminar theory and data in the present analysis existed because the distance from the step edge to the trailing shock was so short that the mixing profile was not fully developed. To obtain a more accurate theoretical calculation, the laminar mixing equations must be solved for the particular flow conditions of the individual problem as indicated in reference 5. Transitional mixing is that in which transition from laminar to turbulent mixing occurred between the step edge and the reattachment point. As expected, the transitional mixing data were between the laminar and the turbulent data. Their location in this range would depend on the location of the transition point with respect to the step edge and the trailing shock.

Reasons that may explain the differences between experiment and theory at other Mach numbers are as follows: At Mach 1.7 the mixing was known to be transitional, and hence the data would be expected to be higher than turbulent theory, as shown in the figure. At Mach 2.3 the initial boundary layer was turbulent, but a reflected shock wave crossed the wake region of the step and probably caused the discrepancy that is shown. At Mach 2.48 the initial boundary layer was laminar, but the nature of the mixing was not determined. Since the data point was a little higher than turbulent theory as at Mach 1.7, it is quite likely that the mixing again was transitional.

The effect of varying step angle at constant initial Mach number is shown in figure 3(b). For these data the initial boundary layer was turbulent and therefore the data are compared only with turbulent theory. There was excellent agreement between experiment and theory at step angles less than 12°, but theory was higher at larger angles. It is possible that this discrepancy was caused by boundary-layer separation ahead of the step, since base pressure had increased above p_0.

Other data exist for which the flow properties were more nearly like those of the flow model (such as in ref. 1), and the agreement between theoretical and experimental base-pressure ratios was better than shown here; but the data discussed previously are of more interest for the present analysis, because pressure distributions downstream of the base were also reported. These pressure distributions are compared with theory for zero step angle in figures 4(a) to (d) and for varying step angle in figures 4(e) to (g). The theoretical pressure distributions were determined for the experimental values of base-pressure ratio (details appear in appendix C). By so doing, the accuracy of the portion of the flow model in the region of this pressure rise could be tested without the influence of possible discrepancies between the theoretical and actual flow in other regions. However, it should be noted that, if the experimental base pressure is not known in advance and the pressure distribution is computed using the theoretical base pressure, then differences between the theoretical and experimental base pressure will affect the accuracy of the pressure-distribution calculation.

With transitional mixing at Mach 1.7 (fig. 4(a)) the experimental distribution agreed fairly well with turbulent theory. As might be expected, the abrupt changes in pressure distribution predicted by the theory were more gradual in the real flow. At Mach 2 (fig. 4(b)) data for turbulent, laminar, and transitional mixing are presented for comparison with turbulent and laminar theory. The turbulent data agree very well with theory, and the laminar data agree well at the beginning and at the end of the pressure rise. The actual rise in the latter case is much more gradual than theory, suggesting again that the mixing profile was not fully developed. As expected, the transitional rise curve was between the laminar and turbulent curves. The agreement was poor at Mach 2.3 (fig. 4(c)), but this probably was due to the interference of the reflected shock wave. With a laminar initial boundary layer at Mach 2.48 (fig. 4(d)), the data were much closer to turbulent than to laminar theory, again indicating that mixing was transitional. With nonzero step angles (figs. 4(e) to (g)), the theoretical pressure rises were located

566131—61——2

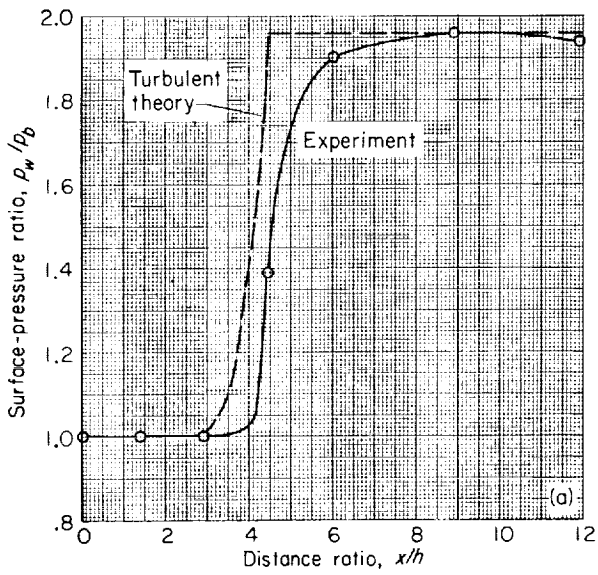

(a) Step angle, τ, 0°; Mach number, 1.7; transitional mixing.

farther downstream than the experimental rise, but the magnitude of the rise was in good agreement. In general, the shapes of these pressure-rise curves differed more from theory than did those for the zero step angle.

AXISYMMETRIC CONFIGURATIONS

Boundary-layer survey.—The flow just upstream of the base of the axisymmetric configurations was surveyed by means of Pitot rakes located in the plane of the struts and normal to it. The results, presented in figure 5(a), show a boundary-layer-thickness ratio δ/d of 0.125. The cause for the discontinuity near the model surface in the profile of the rake normal to the struts is not known, but it could be a result of faulty instrumentation or a shock-wave impingement. Static pressures were measured on the model surface near the base of each rake and, as indicated in the figure, show negligible variation in circumferential

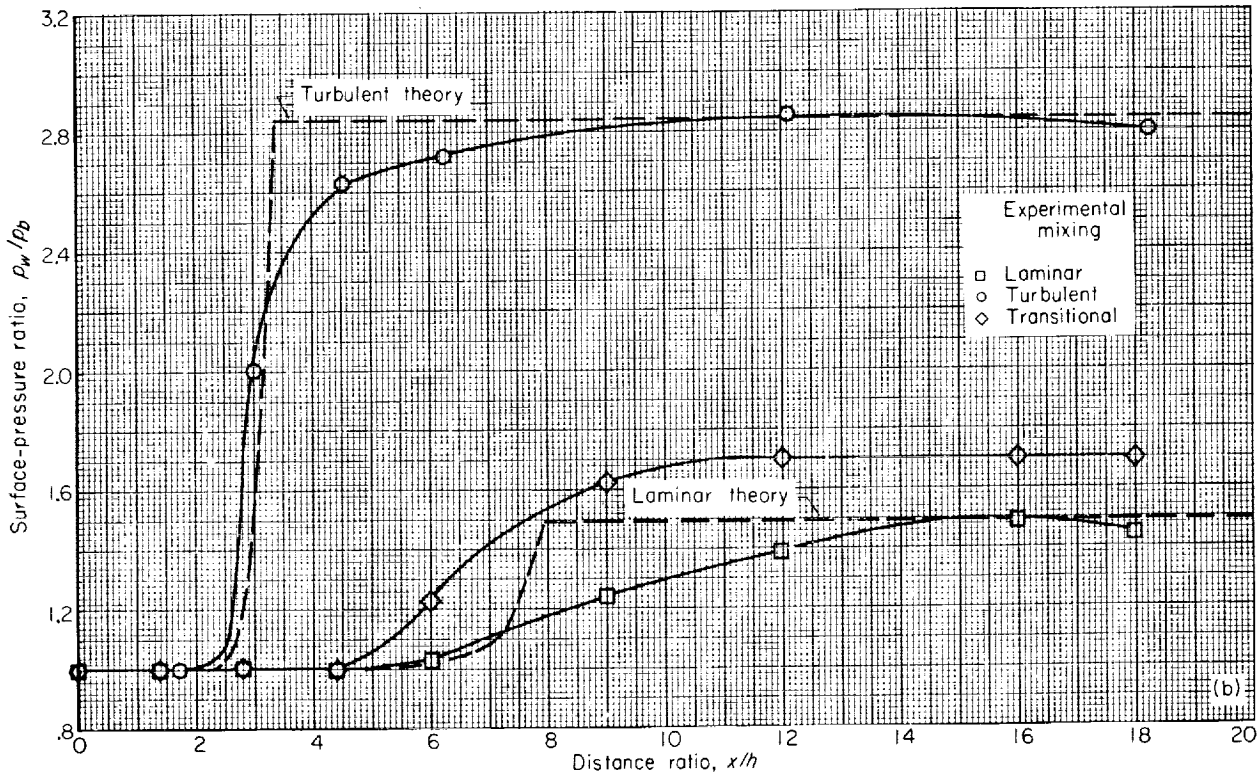

(b) Step angle, τ, 0°; Mach number, 2.0.

FIGURE 4.—Two-dimensional-step pressure distribution.

distribution. Local Mach numbers just outside the body boundary layer were computed from the ratio of model surface static pressure to the Pitot pressure. Results shown in the figure indicate a substantial wake behind the struts. However, this wake probably existed over a relatively small portion of the body circumference, and its presence was neglected in the calculations.

Assuming uniform static pressure along the length of the Pitot rake, these data were used to compute the velocity-ratio profiles presented in figure 5(b). Also shown are theoretical profiles for a flat plate with the same length as the basic body and for both laminar and turbulent flow. The boundary-layer thicknesses were calculated from the following equations of references 9 and 10:

$$\delta_L = \frac{5}{\sqrt{\nu l/u_0}} \text{ and } \delta_T = \frac{0.37l}{\sqrt[5]{u_0 l/\nu}}$$

The laminar profile was obtained from the Blasius

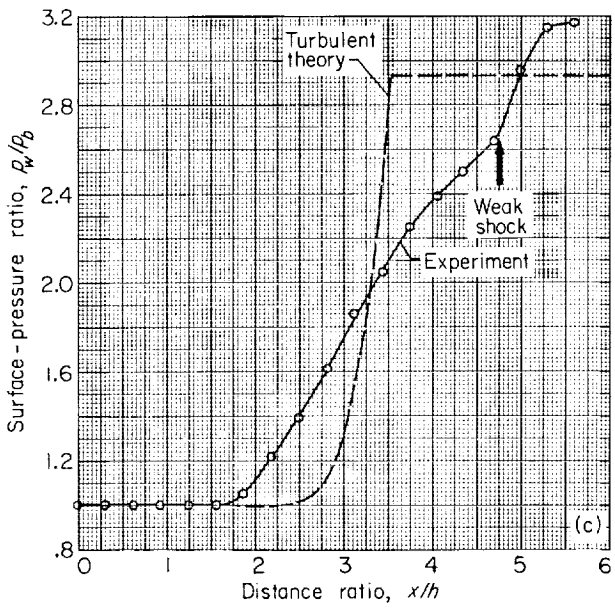

(c) Step angle, τ, 0°; Mach number, 2.3; turbulent mixing.

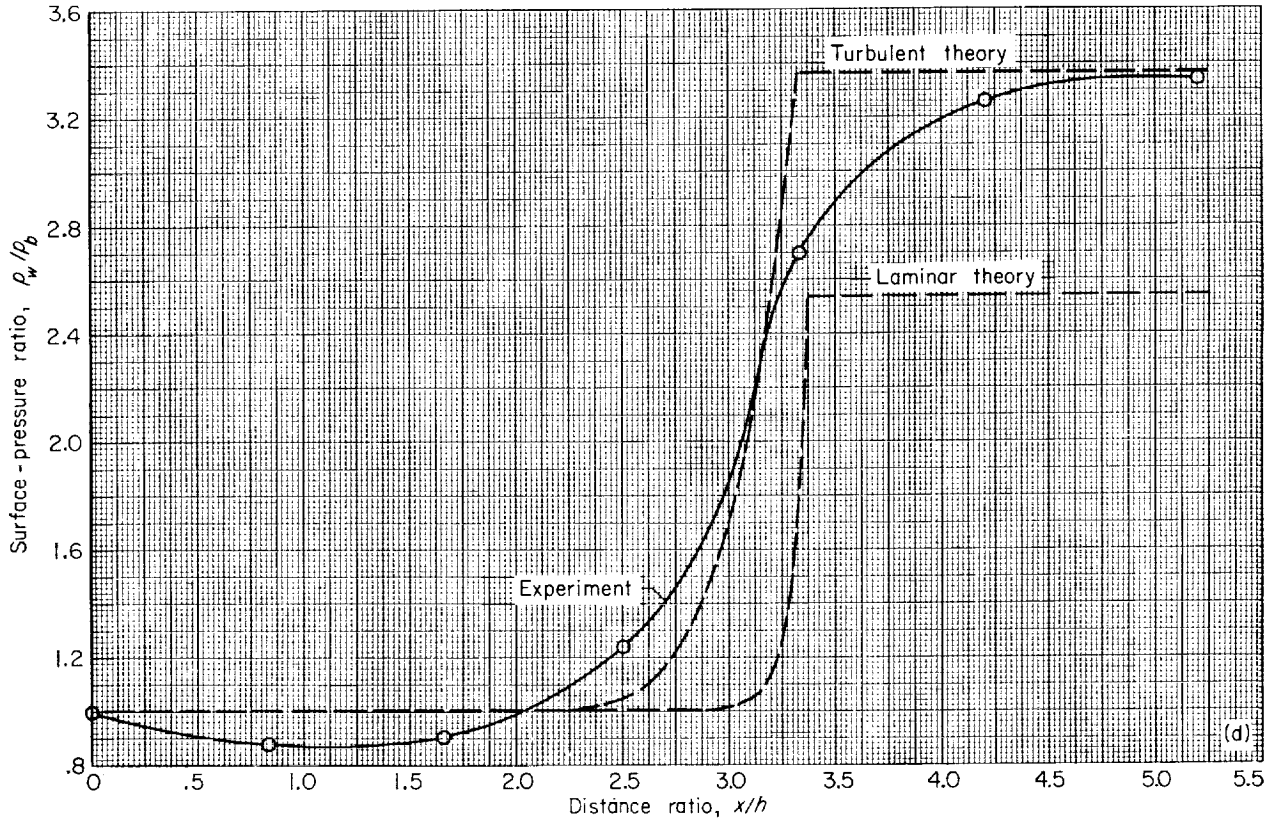

(d) Step angle, τ, 0°; Mach number, 2.48; laminar initial boundary layer.

FIGURE 4.—Continued. Two-dimensional-step pressure distribution.

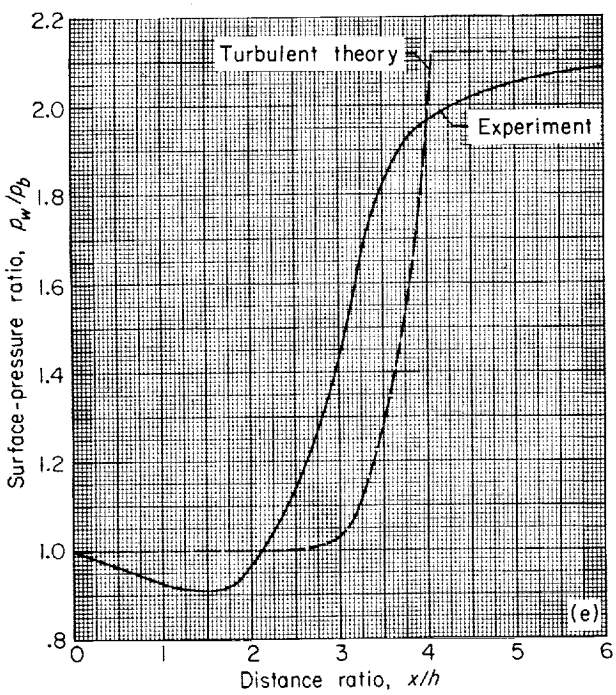

(e) Step angle, τ, 7°; Mach number, 1.86; turbulent mixing.

solution, and the turbulent profile from the equation $u/u_0=(y/\delta)^{1/7}$. The boundary layer was clearly turbulent, and hence the theoretical analyses that follow were made for turbulent mixing.

Cylindrical test bodies.—Schlieren photographs of the flow with cylindrical test bodies are presented in figure 6. The various flow regions considered in the section ANALYTICAL FLOW MODEL are discernible. The fact that some of the test bodies did not extend all the way upstream to the plane of the base of the basic body (see figs. 6(c) and (d)) did not affect the data, because they did extend upstream of the trailing-shock pressure rise.

The experimental and theoretical effects of the size of the cylindrical test bodies on base-pressure ratio are shown in figure 7. Data from several sources are presented, and all showed a similar trend as radius ratio varied; decreasing the ratio from 1 to zero first caused a rapid decrease in base-pressure ratio, then a gradual increase, and finally a slight or negligible increase. The unpublished-data point was obtained with the

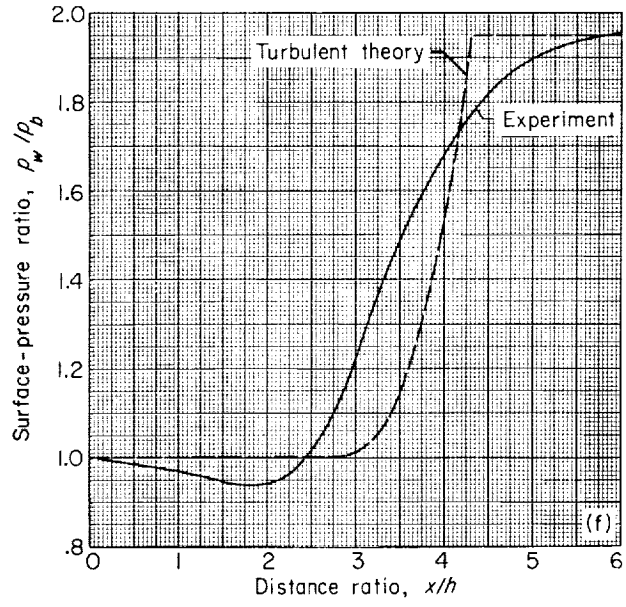

(f) Step angle, τ, 12°; Mach number, 1.86; turbulent mixing.

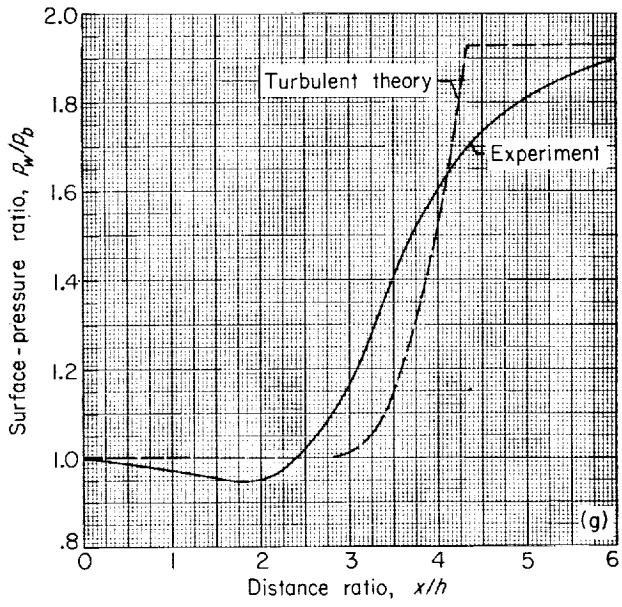

(g) Step angle, τ, 16½°; Mach number, 1.86; turbulent mixing.

FIGURE 4.—Concluded. Two-dimensional-step pressure distribution.

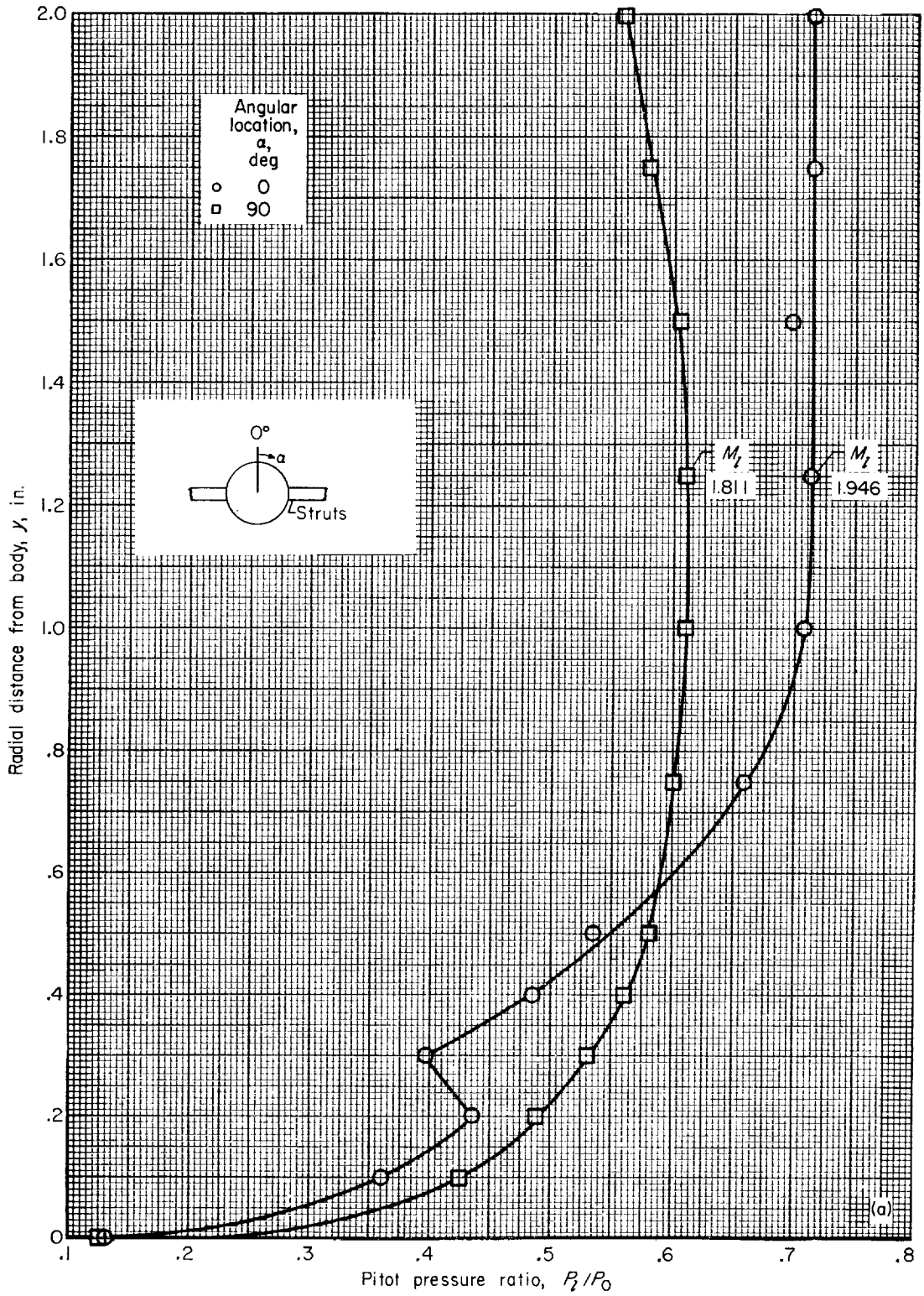

(a) Pitot pressure profiles.

FIGURE 5.—Boundary-layer survey. Mach number, 1.98.

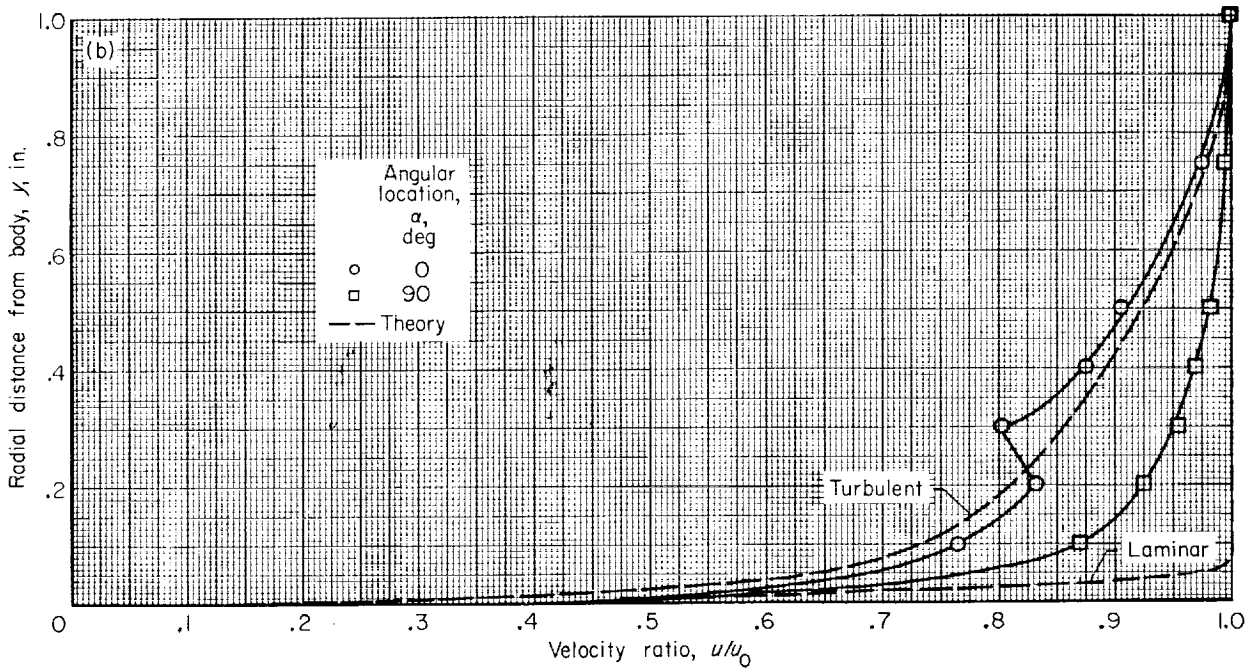

(b) Velocity profiles.

FIGURE 5.—Concluded. Boundary-layer survey. Mach number, 1.98.

same support struts and in the same part of the tunnel test section (the supersonic section) as the present study and agreed closely with the present data.

There was a good deal of scatter in these data, and possible reasons for this scatter are as follows:

The data of reference 11 were obtained with different struts in the transonic portion of the test section and indicate a lower base-pressure ratio than the present study. This decrease may have been due to a changed strut effect and/or to a change in tunnel flow properties, since the flow upstream of the base was more uniform in the supersonic than in the transonic section.

The results of reference 3 were obtained in free flight with zero radius ratio and in a different facility using a sting support rather than struts with other radius ratios. These data also showed generally lower base pressures than the present study. Several factors may have contributed to this difference. The model of reference 3 was constructed of a single piece of metal, whereas the present model was constructed of several jointed pieces and also included ducting to allow a base-bleed study. In this latter case there is a possibility that air leaks existed that caused inadvertent base bleed. As has been shown (e.g., ref. 1), small amounts of base bleed produce relatively large increases in base pressure. If present, it impaired the usefulness of the base-pressure-ratio data but not that of the pressure-distribution data. Another factor contributing to this difference may have been differences in the initial boundary layer. It probably was thinner in reference 3 than for the present study, since the effect of a lower Reynolds number was more than offset by the shorter length of the basic body. (Values of these parameters are indicated on the figure.) With the thinner boundary layer, the mixing profile may have been closer to being fully developed ahead of the trailing shock, and lower base pressures would result. A third factor contributing to this difference may be that a strut effect was nonexistent for most of the data from reference 3. Thus, the base-pressure data of reference 3 probably are more significant than those of the present test.

The theoretical curves are shown in figure 7 for the two cases of a plane and of a conical trailing shock wave. Details of these calculations are discussed in appendix B. In its simplified form, the theory can only be used to predict a range of base-pressure ratio for values of radius ratio greater than 0.2 within which the experimental base-pressure ratios may be expected to occur.

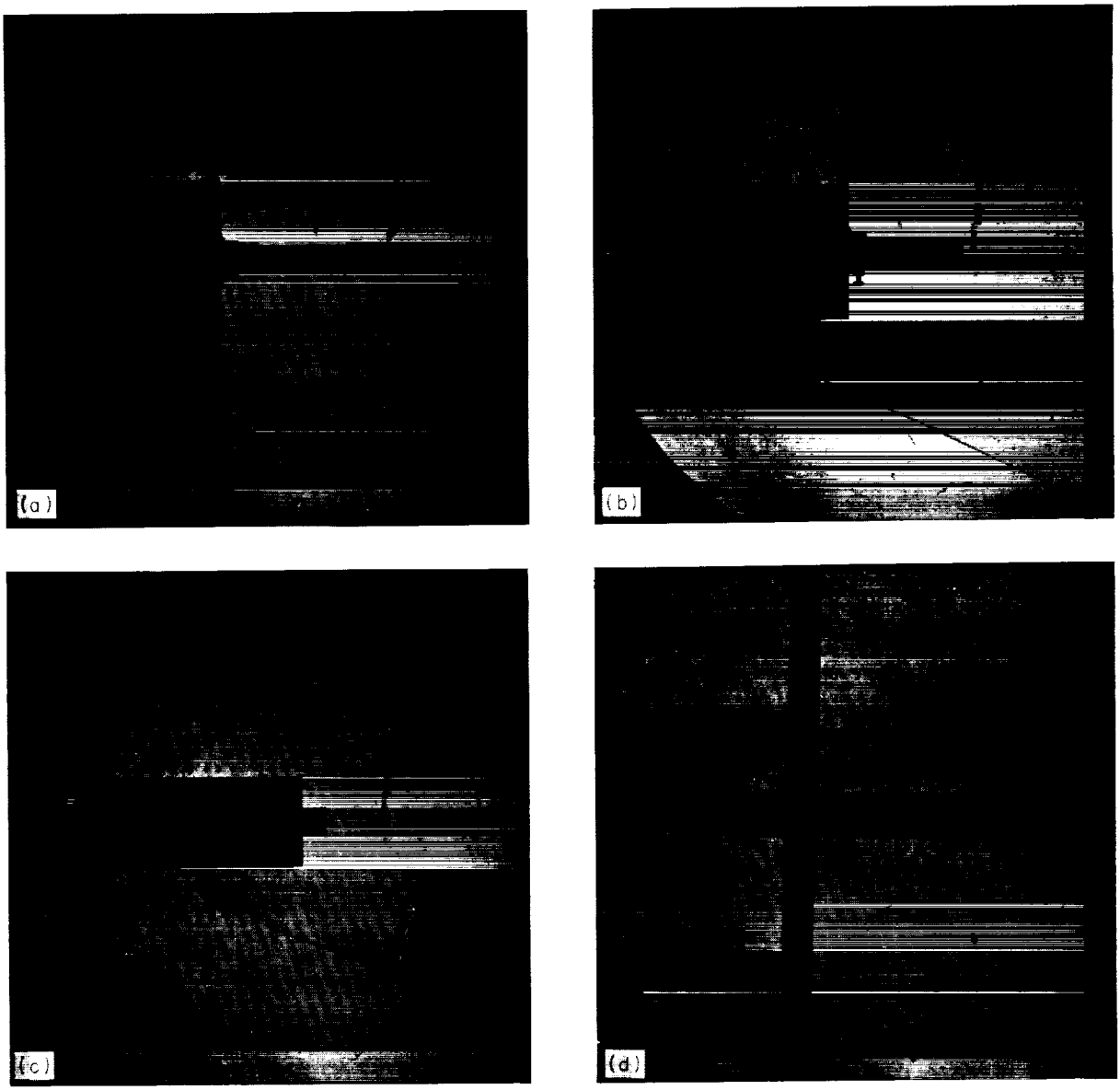

(a) Radius ratio, r/R, 0.875.
(b) Radius ratio, r/R, 0.75.
(c) Radius ratio, r/R, 0.5.
(d) Radius ratio, r/R, 0.25.

FIGURE 6. Schlieren photographs of flow with cylindrical test bodies. Mach number, 1.98.

A comparison of the experimental and theoretical base-pressure ratio of figure 7 can be better understood by simultaneously analyzing the static-pressure distributions on the test-body surfaces. The experimental and theoretical distributions of the present test are presented in figure 8. The theoretical calculations are presented in appendix C in detail and, as for the two-dimensional configurations, were made for the experimental value of base-pressure ratio. These data show that, at radius ratio 0.875 (fig. 8(a)), the trailing-shock pressure rise was very close to the plane-shock value; at radius ratio 0.75 (fig. 8(b)), it was midway between that of the plane and the conical shocks; and, at radius ratio 0.5 (fig. 8(c)), it was equal to the conical-shock value. Thus, the trailing shock was effectively a plane wave at large values of radius ratio and weakened, approaching conical-shock strength, as radius ratio decreased. It would be expected, then, that the experimental

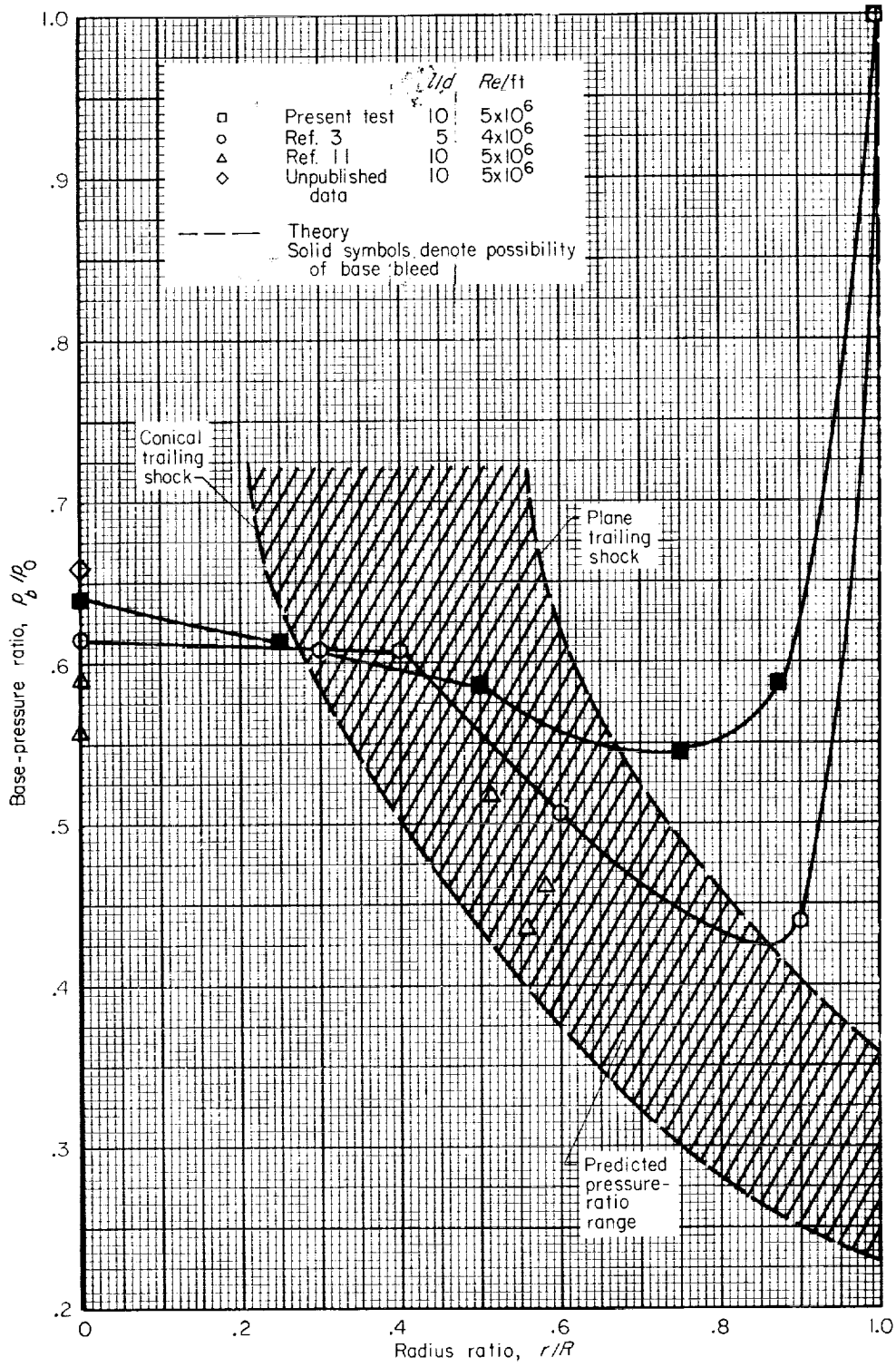

FIGURE 7.—Effect of cylinder size on base-pressure ratio. Mach number, 1.98.

base-pressure ratios of figure 7 would cross over the predicted range from the plane shock toward the conical-shock value as radius ratio decreased. The data between radius ratios of about 0.9 and 0.4 clearly showed this trend, particularly for the data of reference 3. At radius ratio greater than about 0.9, the data deviated markedly from this trend because of the effect of the initial boundary layer; that is, the mixing length was insufficient to allow a fully developed profile.

For axisymmetric configurations such that the base-pressure ratio is less than 1.0, the free streamline curves toward the flow axis. Since there is a limit to the strength of the trailing shock, the free streamline would not intersect the test-body surface if the required flow deflection exceeded this limit. Thus, it is possible that a minimum effective radius ratio exists and that base pressure is independent of test-body geometric radius ratio for values less than this minimum. Data of reference 12 indicate that base pressure is affected by radius ratio over the entire range, but that at high Reynolds numbers comparable to the present study the effect at small values of radius ratio is not large. Since this concept of a minimum wake size is a useful one, it was employed in the present analysis.

For the data of figure 7 the minimum wake radius ratio was between 0.4 and 0.5. Minimum wake sizes measured from shadowgraph photos of free-flight bodies are presented in reference 3 over a range of free-stream Mach number; these data indicate a minimum radius ratio of 0.55 for the Mach number of the present study and hence are in fair agreement with figure 7. The theoretical calculations show a minimum radius ratio of about 0.55 for a plane trailing shock and a minimum of about 0.2 for a conical shock, thus bracketing the experimental results.

The pressure distribution on a cylindrical test body with a radius ratio less than the minimum wake size is shown in figure 8(d). If the physical radius ratio of 0.25 is used in the theoretical calculation of pressure distribution, the results do not agree with the data, as shown in the figure. If the minimum wake radius ratio of 0.5 is used as the effective test-body size, the results are in much better agreement and hence should be used.

The magnitudes and locations of the experimental and theoretical pressure rises on the cylindrical test bodies are summarized in figure 9. Figure 9(a) clearly shows the weakening of the trailing shock from a plane to a conical strength as the radius ratio decreased from 0.875 to 0.5. It is not apparent how to predict the strength of this shock wave at intermediate values of radius ratio, but as a first approximation it could be as-

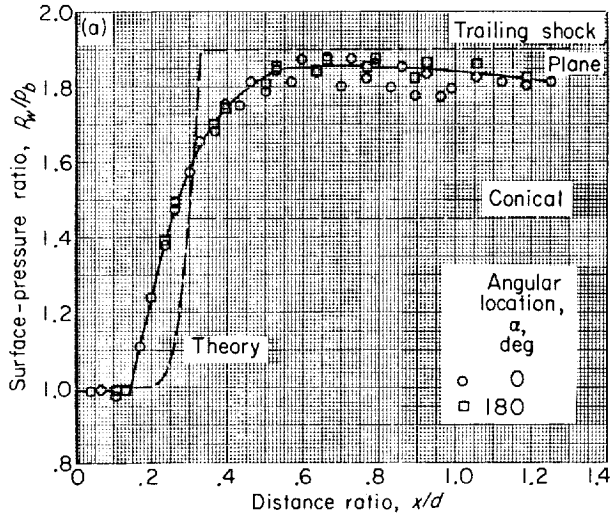

(a) Radius ratio, r/R, 0.875.

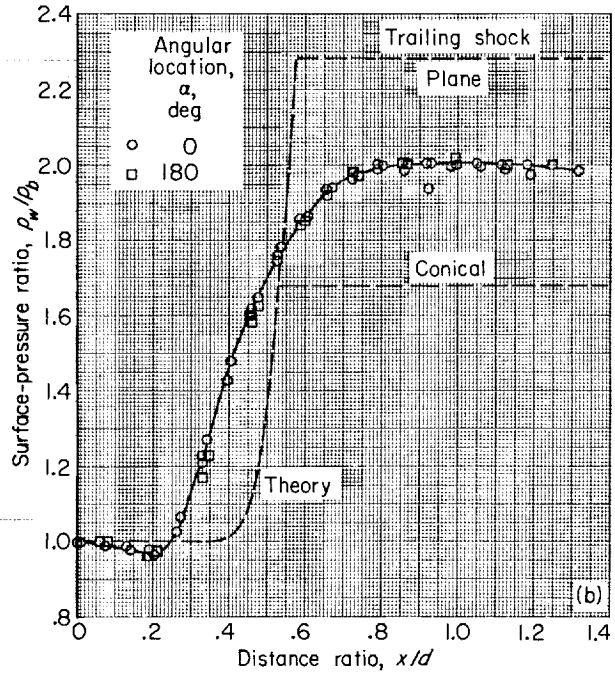

(b) Radius ratio, r/R, 0.75.

FIGURE 8. Cylindrical-body pressure distribution. Mach number, 1.98.

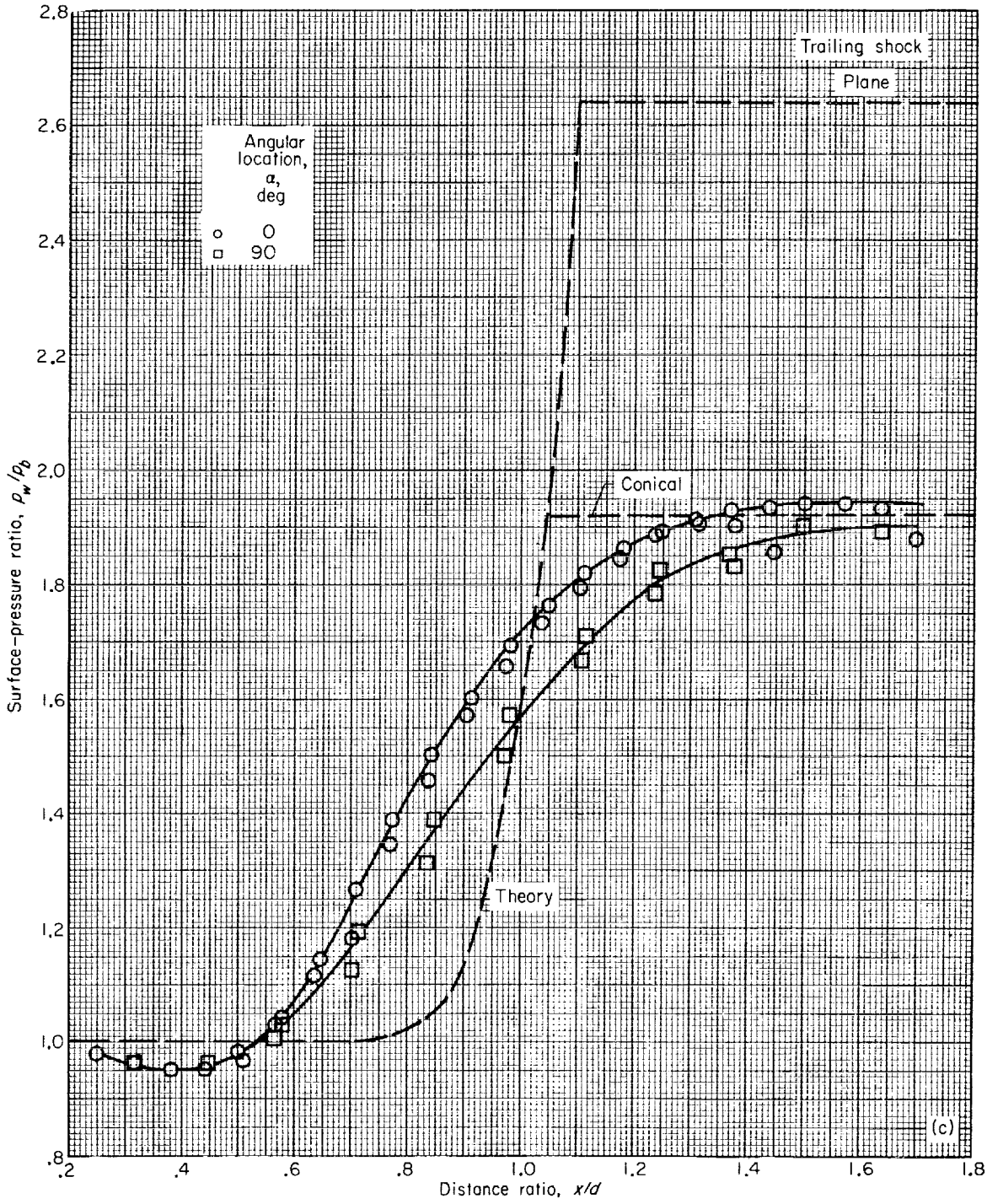

(c) Radius ratio, r/R, 0.5.

FIGURE 8.—Continued. Cylindrical-body pressure distribution. Mach number, 1.98.

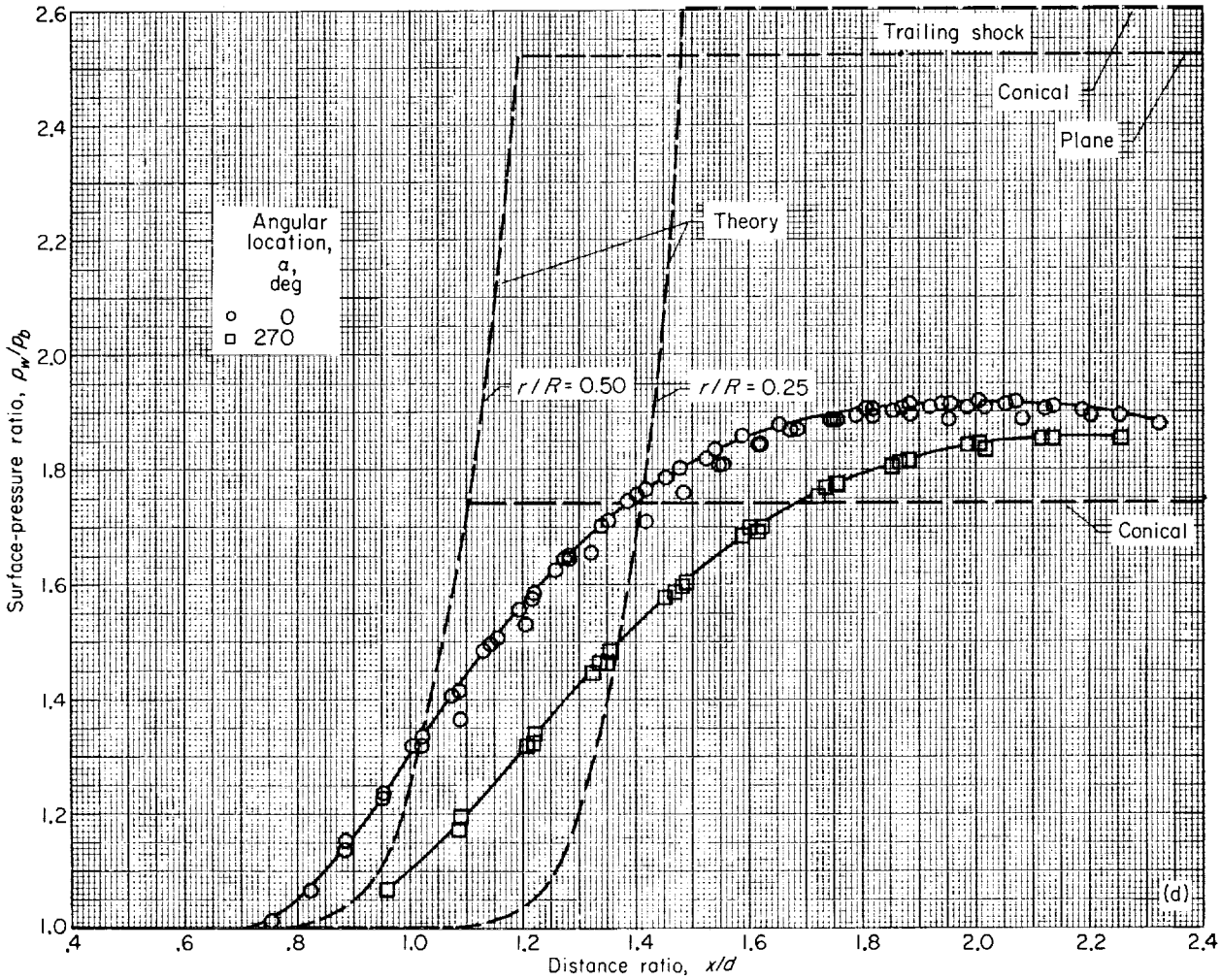

(d) Radius ratio, r/R, 0.25.

FIGURE 8.—Concluded. Cylindrical-body pressure distribution. Mach number, 1.98.

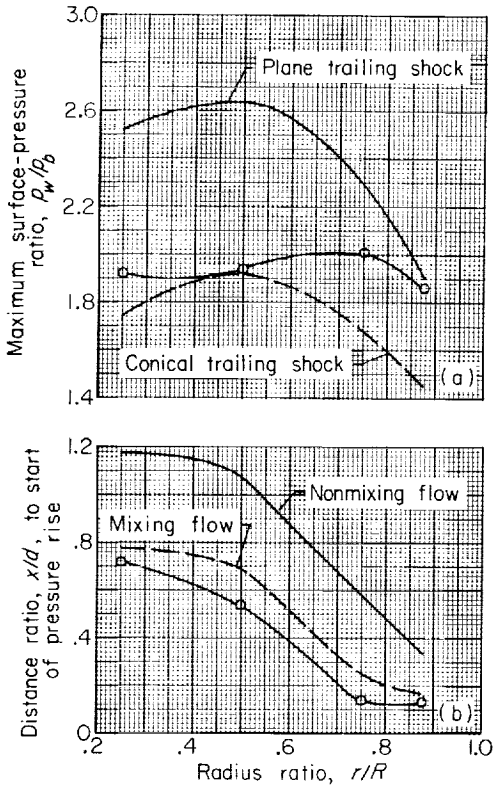

(a) Magnitude of pressure rise.
(b) Location of pressure rise.

FIGURE 9.—Summary of location and magnitude of pressure rise on cylindrical test bodies. Mach number, 1.98.

sumed to be constant at about 1.9 for the free-stream Mach number of 2. The variation of this shock strength with stream Mach number was not determined in this study. The location of the start of the pressure rise is shown in figure 9(b). Neglecting the effect of mixing and assuming that the pressure rise began where the free streamline intersected the test-body surface (a Prandtl-Meyer expansion followed by three-dimensional nonmixing flow) produced a theoretical location that was well downstream of the experimental location, as shown in the figure. However, by including the effect of mixing, the theory was in fairly good agreement with the data.

One thing that the theory did not do well was to predict the shape of the pressure-rise curve accurately with large steps. As shown in figure 8, the experimental curve rose more sharply initially and then leveled off more gradually. In all cases the experimental distance required to complete the pressure rise was greater than theory. This difference increased as radius ratio decreased. Reasons for the discrepancy are that the theory assumed a fully developed profile that may not actually be achieved and also neglected local flow effects along the test-body surface. Figures 8(c) and (d) show that the pressure rise in the wake of the struts was more gradual than in the normal plane.

Conical test bodies.—Schlieren photographs of the flow with the conical test bodies are presented in figure 10. As with the cylindrical test bodies, the various regions of flow described in the section ANALYTICAL FLOW MODEL are apparent. Again, all of the data were obtained so that the test body extended upstream of the trailing-shock pressure rise.

The experimental and theoretical effects of radius ratio on base-pressure ratio are presented in figure 11 for cone angles of 15° and 25°. The theoretical calculations are described in appendix B. As expected, the overall level of base-pressure ratio was higher with the larger cone angle. The predicted range of base-pressure ratio unfortunately was rather large, particularly with the large cone angle at large values of radius ratio. All the data fell within the predicted range. As with the cylindrical-test-body data, there was a possibility that inadvertent base bleed had occurred. A change in experimental procedure that reduced this possibility was made for a portion of the 25°-cone data; and, as shown in the figure by the open symbols, base-pressure ratio was reduced somewhat. The base-pressure data with the 25° cone showed the same trend as radius ratio was decreased as did the cylindrical data; that is, the data crossed over the predicted range from near the plane-shock value toward the conical-shock value. However, the 15°-cone data did not show this trend.

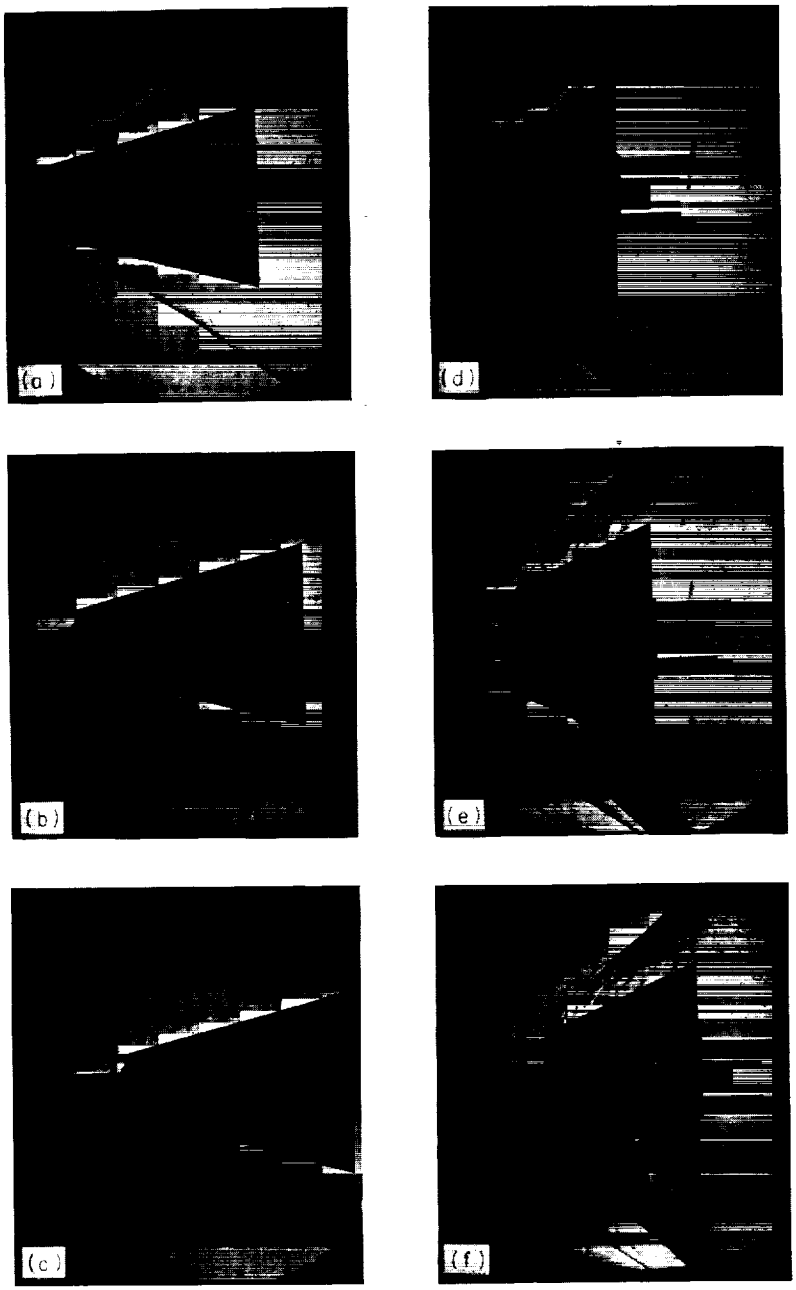

(a) Radius ratio, r/R, 0.475; half cone angle, τ, 15°.
(b) Radius ratio, r/R, 0.31; half cone angle, τ, 15°.
(c) Radius ratio, r/R, 0.125; half cone angle, τ, 15°.
(d) Radius ratio, r/R, 0.715; half cone angle, τ, 25°.
(e) Radius ratio, r/R, 0.425; half cone angle, τ, 25°.
(f) Radius ratio, r/R, 0.122; half cone angle, τ, 25°.

FIGURE 10.—Schlieren photographs of flow with conical test bodies. Mach number, 1.98.

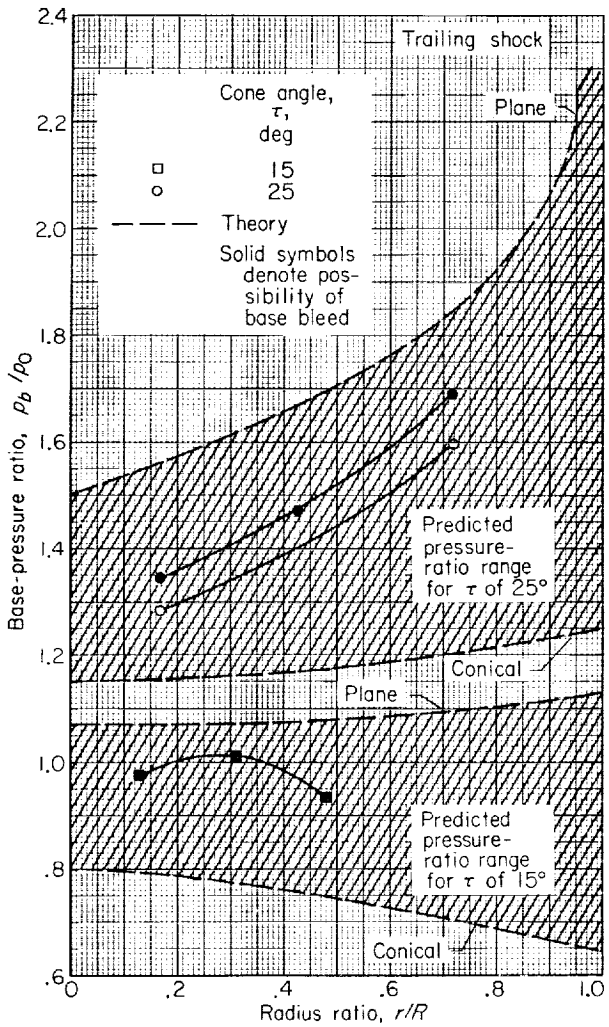

FIGURE 11.—Effect of cone geometry on base-pressure ratio. Mach number, 1.98.

The experimental and theoretical test-body surface-pressure distributions appear in figure 12. The theoretical calculations are described in detail in appendix C and again were made for the experimental value of base-pressure ratio. In all cases the magnitude of the trailing-shock pressure rise was somewhat greater than for a conical shock. Differences between theoretical and experimental pressure distribution were similar to those for the cylindrical test bodies.

The magnitudes of the experimental and theoretical trailing-shock pressure rises and the locations of the start of the rises are summarized in figure 13. For both cones the magnitude of the experimental pressure rise was about 0.2 greater than conical-shock theory (fig. 13(a)) regardless of radius ratio. This fact appears to contradict the trend shown in figure 11 for the 25° cone, where experiment is closer to plane-shock theory at high radius ratios and closer to conical theory at lower radius ratios. The reason for this discrepancy is not apparent. As shown in figure 13(b), the theoretical location of the start of the pressure rise was seriously in error if the effect of mixing was neglected (as described for the cylindrical test bodies); but if it was included, the agreement between the data and theory was good, especially with the 25° cone.

Effects of base bleed.—The possibility that inadvertent base bleed occurred during the present test has already been discussed. Experimental and theoretical effects of deliberate base bleed on base-pressure ratio with the cylindrical test bodies are shown in figure 14. Details of the theoretical calculations appear in appendix D. Calculations for both a plane and a conical trailing shock were made at radius ratios of 0.875 and 0.75 (figs. 14(a) and (b)), but for lower values of radius ratio only a conical-shock solution was possible. For radius ratios less than the minimum wake size (figs. 14(d) and (e)), the theoretical calculations were made assuming an effective radius ratio of 0.5 as was done earlier for figure 8(d). The magnitude of the experimental base-bleed ratio for values less than 0.1 is questionable, because the method of measuring the flow rate was less accurate at low flow rates. The minimum value of bleed flow was obtained with the control valve closed, and these data points are those presented in figure 7. Thus, figure 14 indicates that some valve leakage occurred for these data, but the flow rate is not accurately known.

The data of figure 14 indicate reasonably close agreement with theory for bleed-flow ratios up to about 0.3, but at higher flow rates the data were

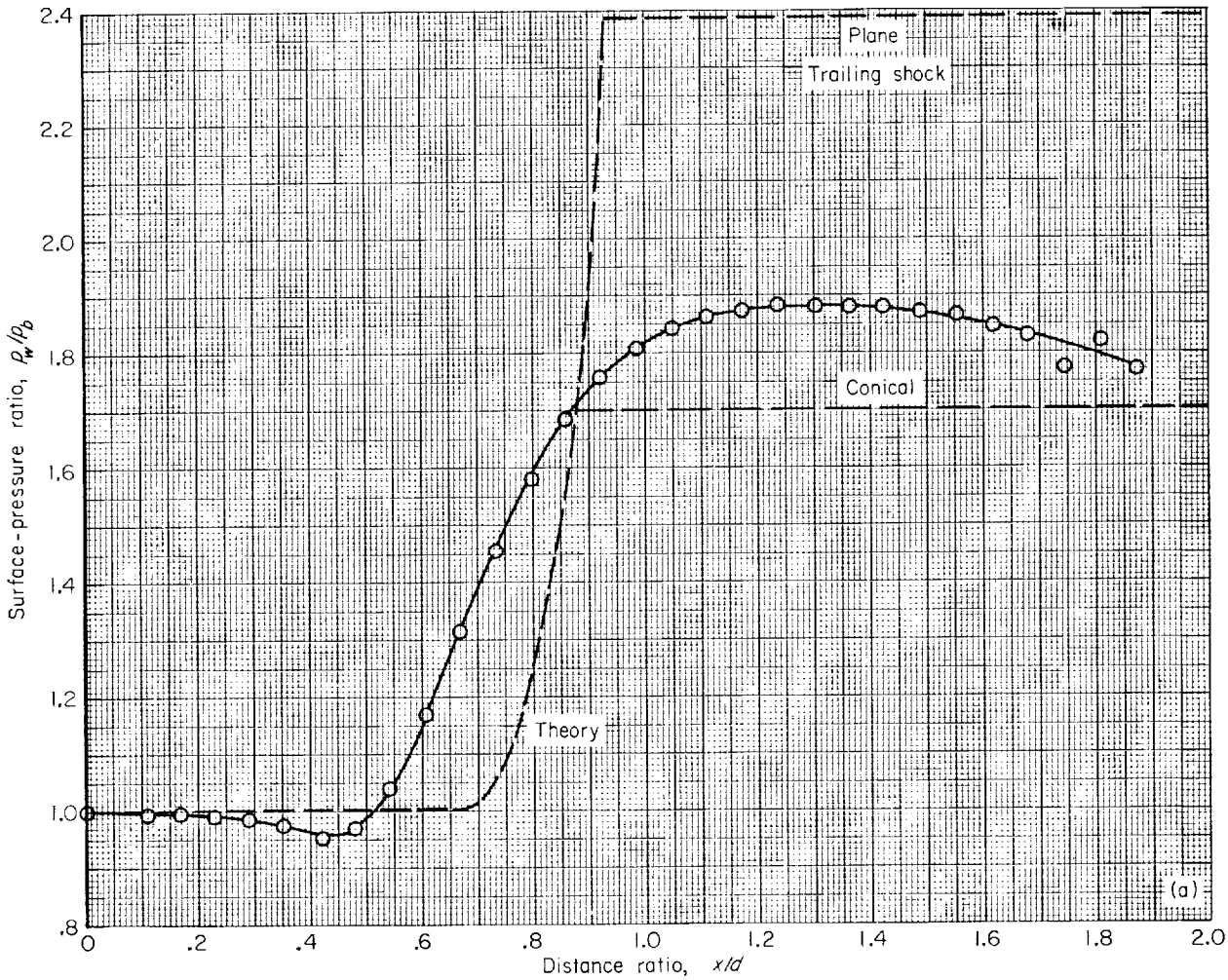

(a) Conical half-angle, 15°; radius ratio, r/R, 0.475; angular location, α, 0°.

FIGURE 12.—Conical-body pressure distribution. Mach number, 1.98.

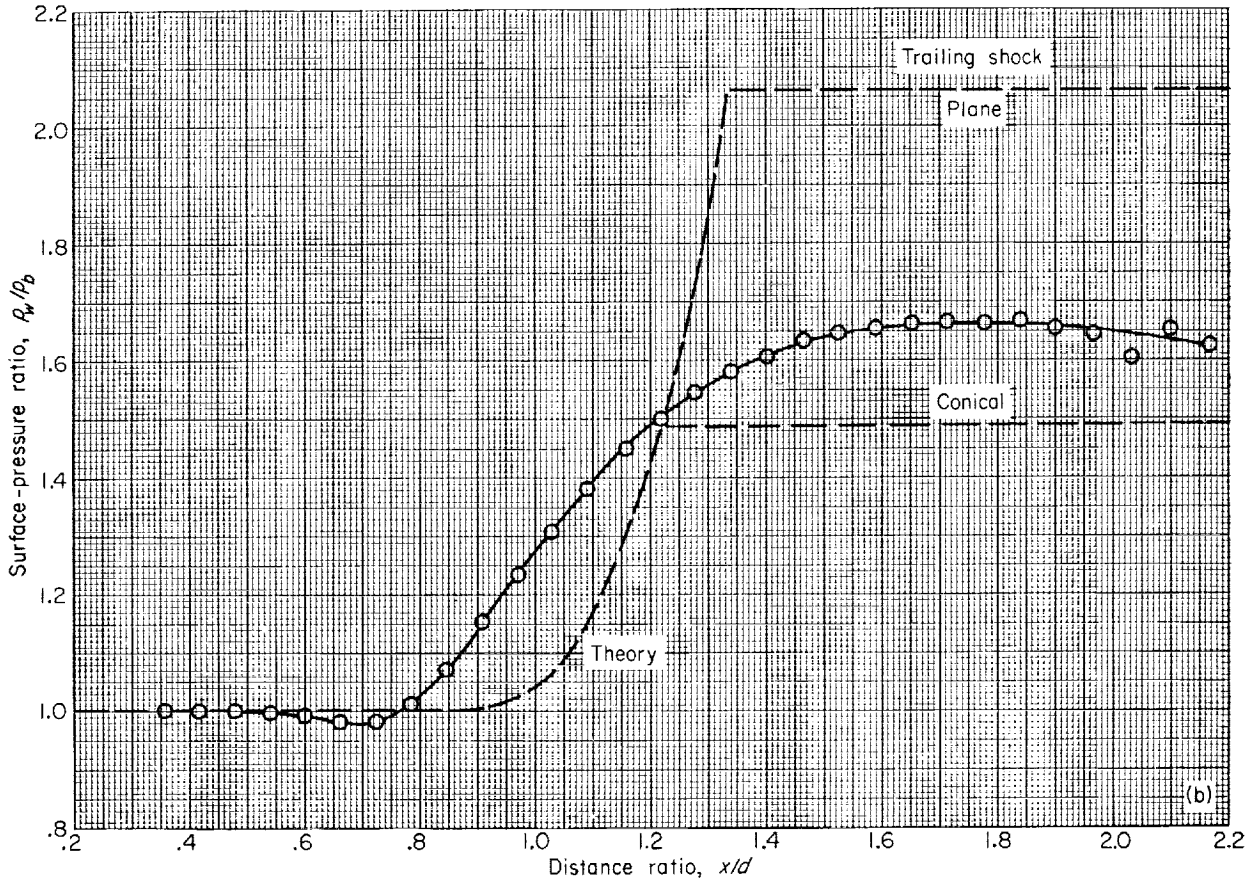

(b) Conical half-angle, 15°; radius ratio, r/R, 0.31; angular location, α, 0°.

FIGURE 12.- Continued. Conical-body pressure distribution. Mach number, 1.98.

less than theory. The reason for this inaccuracy was that the theory neglected the effects of bleed-flow axial momentum, which became increasingly important as flow rate increased. Reference 13 has shown that the effect of bleed momentum is such as to decrease base-pressure ratio and thus is in accord with the present results. In figure 14(e) the bleed flow was varied over an extra-wide range. The resulting variations in base-pressure ratio are similar to those described in reference 14 for a two-dimensional configuration. No attempt was made in the present study to compute a theoretical curve for these moderate and high bleed-flow rates as was done in reference 14, but apparently it could be done.

The effect of base bleed on base-pressure ratio with the conical test bodies is shown in figure 15. For these data the largest value of radius ratio that was investigated with each cone was used. The trends of the effect of base bleed were similar to those for cylindrical test bodies, and the accuracy of base-bleed ratios at values less than 0.1 was still questionable. It is apparent that the difference between theory and experiment increased more rapidly at high bleed flows than it did for the cylindrical test bodies. At base-bleed ratios less than 0.15 all of the data fell within the predicted pressure-ratio ranges; however, the magnitude of the predicted pressure-ratio range became quite large for the higher cone angle at low values of base-bleed ratio, thus decreasing the usefulness of the theoretical calculations.

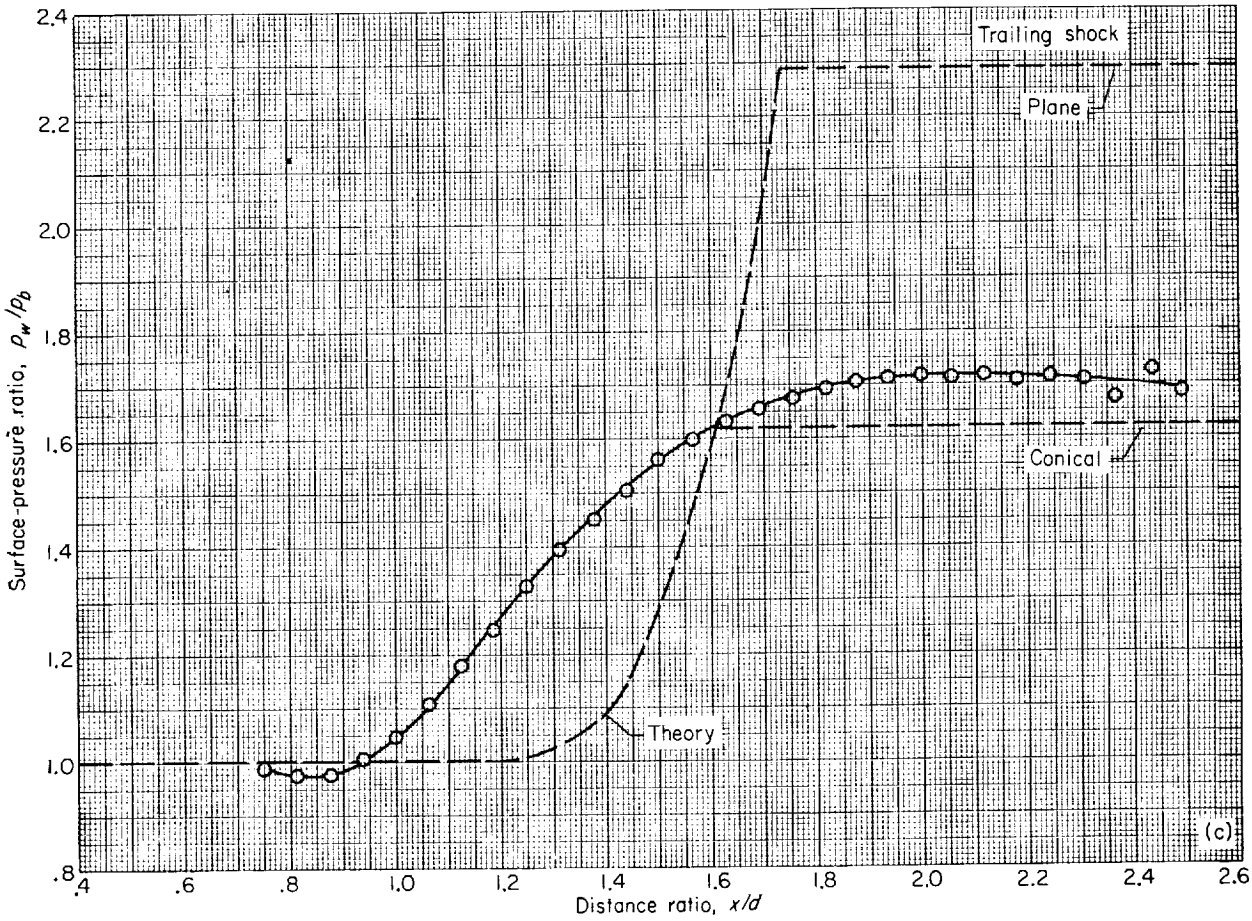

(c) Conical half-angle, 15°; radius ratio, r/R, 0.125; angular location, α, 0°.

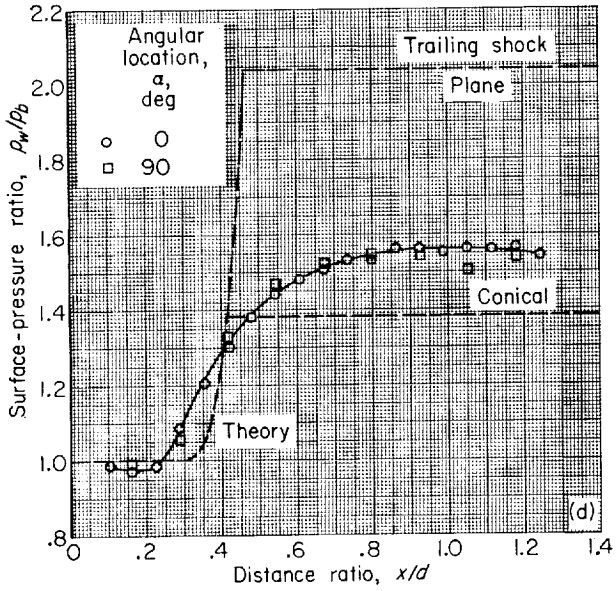

(d) Conical half-angle, 25°; radius ratio, r/R, 0.715.

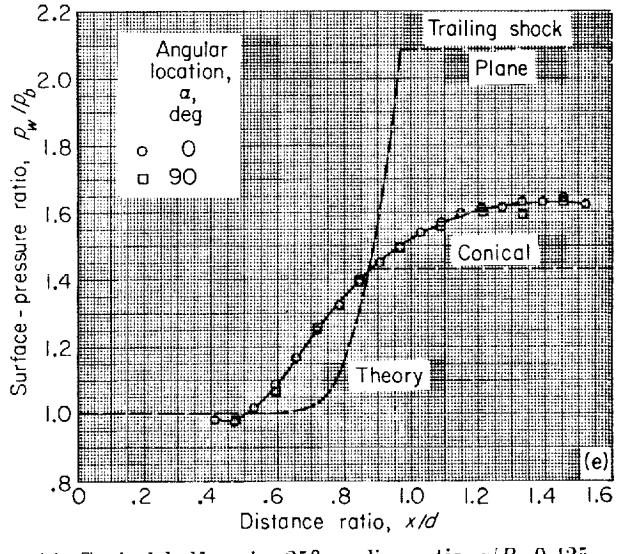

(e) Conical half-angle, 25°; radius ratio, r/R, 0.425.

FIGURE 12.—Continued. Conical-body pressure distribution. Mach number, 1.98.

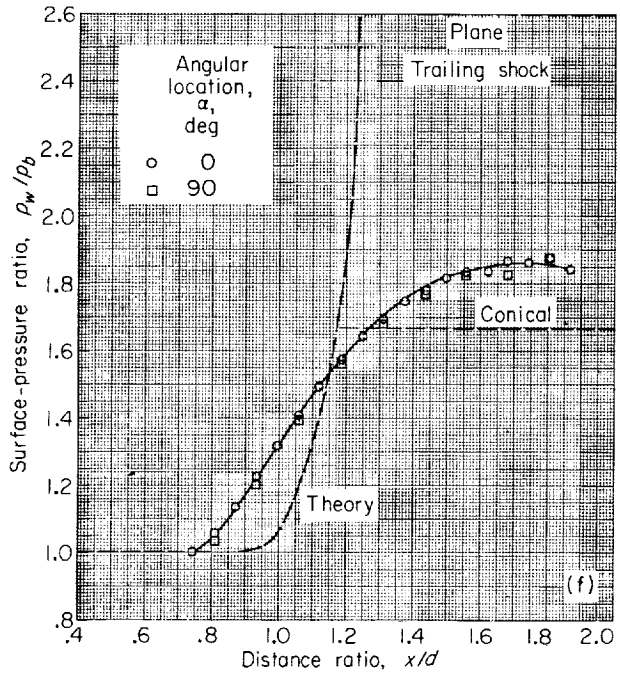

(f) Conical half-angle, 25°; radius ratio, r/R, 0.122.

FIGURE 12. Concluded. Conical-body pressure distribution. Mach number, 1.98.

SUMMARY OF RESULTS

A theoretical and experimental investigation has been conducted of the pressure distribution on the surface of a circular cylinder or a truncated cone located within the base region of another circular cylinder. A similar analysis of pressure distribution was made for rearward-facing two-dimensional steps, and theoretical results were compared with experimental results of earlier investigations. Effects of base bleed were also studied with the axisymmetric configurations. The following results were obtained:

1. The base-flow theory of references 1 and 2 was used successfully to calculate the base pressures of two-dimensional steps. By approximating three-dimensional flow effects, the same theory was used to predict a range of base pressures for axisymmetric configurations within which the experimental results were expected to occur. The data generally followed the trends predicted by the theory, and deviations apparently could be explained.

2. For two-dimensional steps the magnitude of the pressure rise on the surface downstream of the step could be predicted accurately. The location of the start of the pressure rise and the shape of the pressure-rise curve were closer to theory with zero than with nonzero step angles, and in all cases the distance required to complete the pressure rise was greater than theory.

3. For axisymmetric configurations with cylindrical test bodies, the magnitude of the pressure rise on the test-body surface was nearly constant at about 1.9 for radius ratios less than 0.875. At a radius ratio of 0.875 this pressure rise corresponded to that of a plane trailing shock, and at a radius ratio of 0.5 it corresponded to that for a conical shock. With conical test bodies the pressure rise was about 0.2 greater than that for a conical trailing shock regardless of radius ratio. In all cases the start of the pressure rise was slightly upstream of theory, and the distance required to complete the pressure rise was greater than theory. The shape of the pressure-rise curve differed more from theory at low values of radius ratio than at high values, and in all cases leveled off more gradually than theory.

4. The effects of base bleed on base-pressure ratio for the axisymmetric configurations could be predicted with fair accuracy at bleed-flow ratios less than 0.3 for cylindrical test bodies and less than 0.15 for conical test bodies. A more refined analysis would be required at high bleed flows.

LEWIS RESEARCH CENTER
NATIONAL AERONAUTICS AND SPACE ADMINISTRATION
CLEVELAND, OHIO, *March 31, 1960*

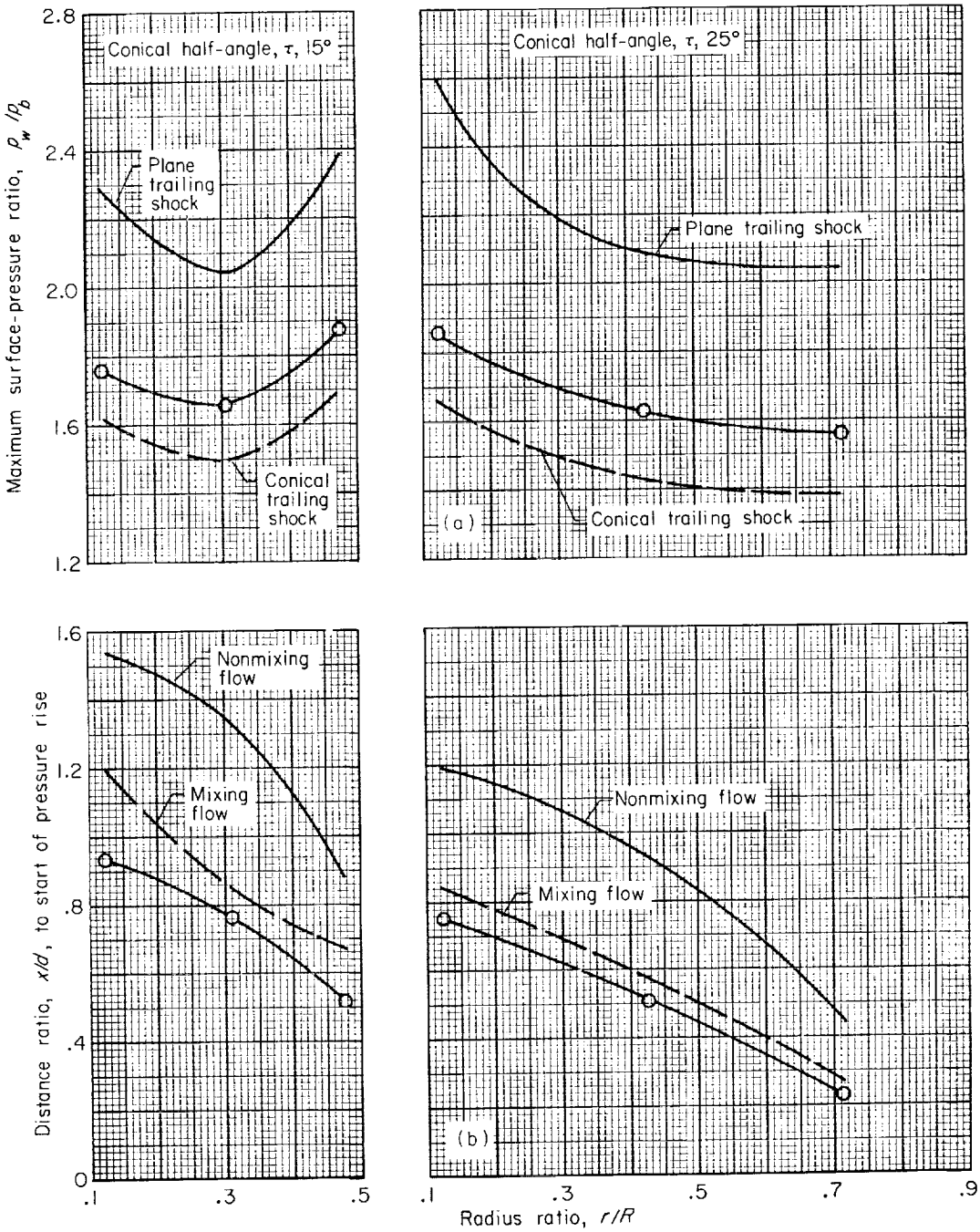

(a) Magnitude of pressure rise.
(b) Location of pressure rise.

FIGURE 13.—Summary of location and magnitude of pressure rise on conical test bodies.

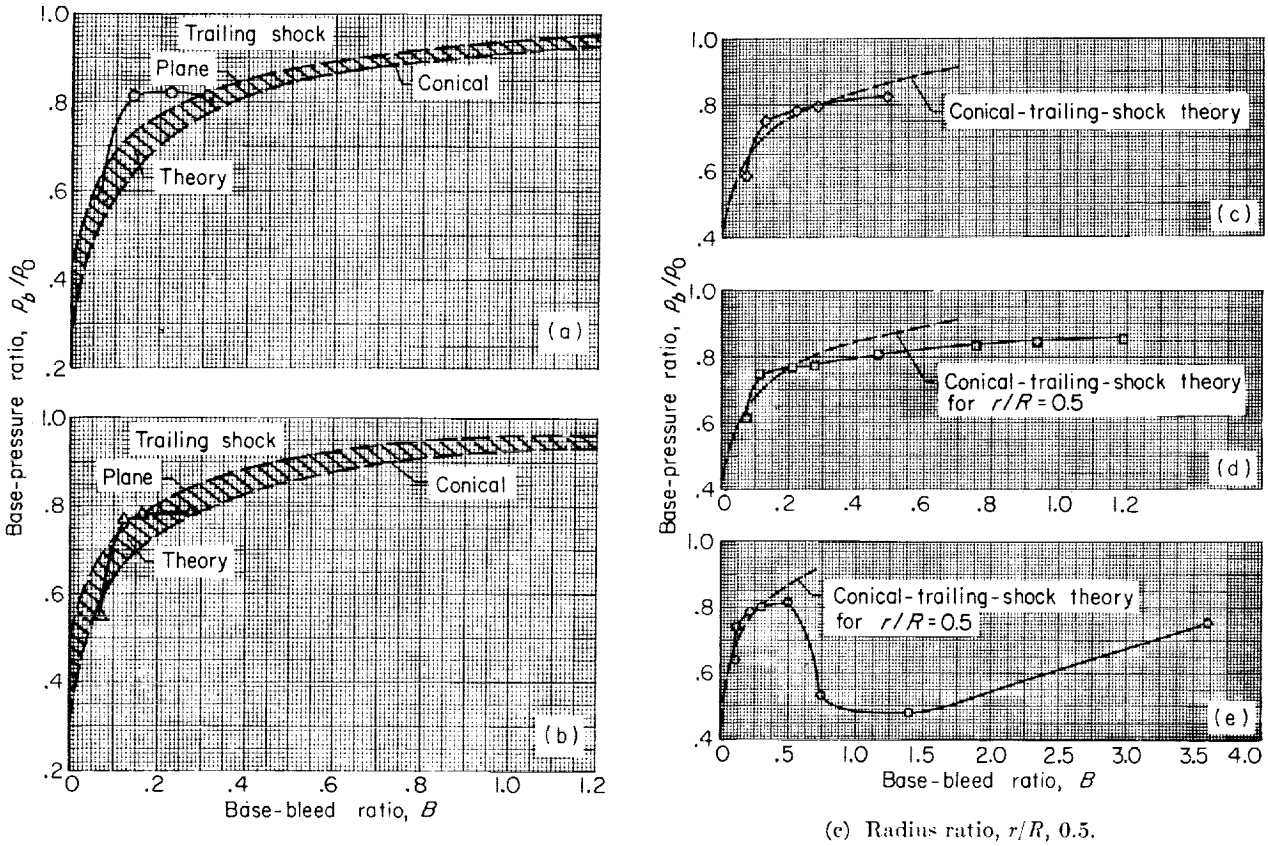

(a) Radius ratio, r/R, 0.875.
(b) Radius ratio, r/R, 0.75.
(c) Radius ratio, r/R, 0.5.
(d) Radius ratio, r/R, 0.25.
(e) Radius ratio, r/R, 0.

FIGURE 14.—Effect of base bleed on base pressure with cylindrical test bodies. Mach number, 1.98.

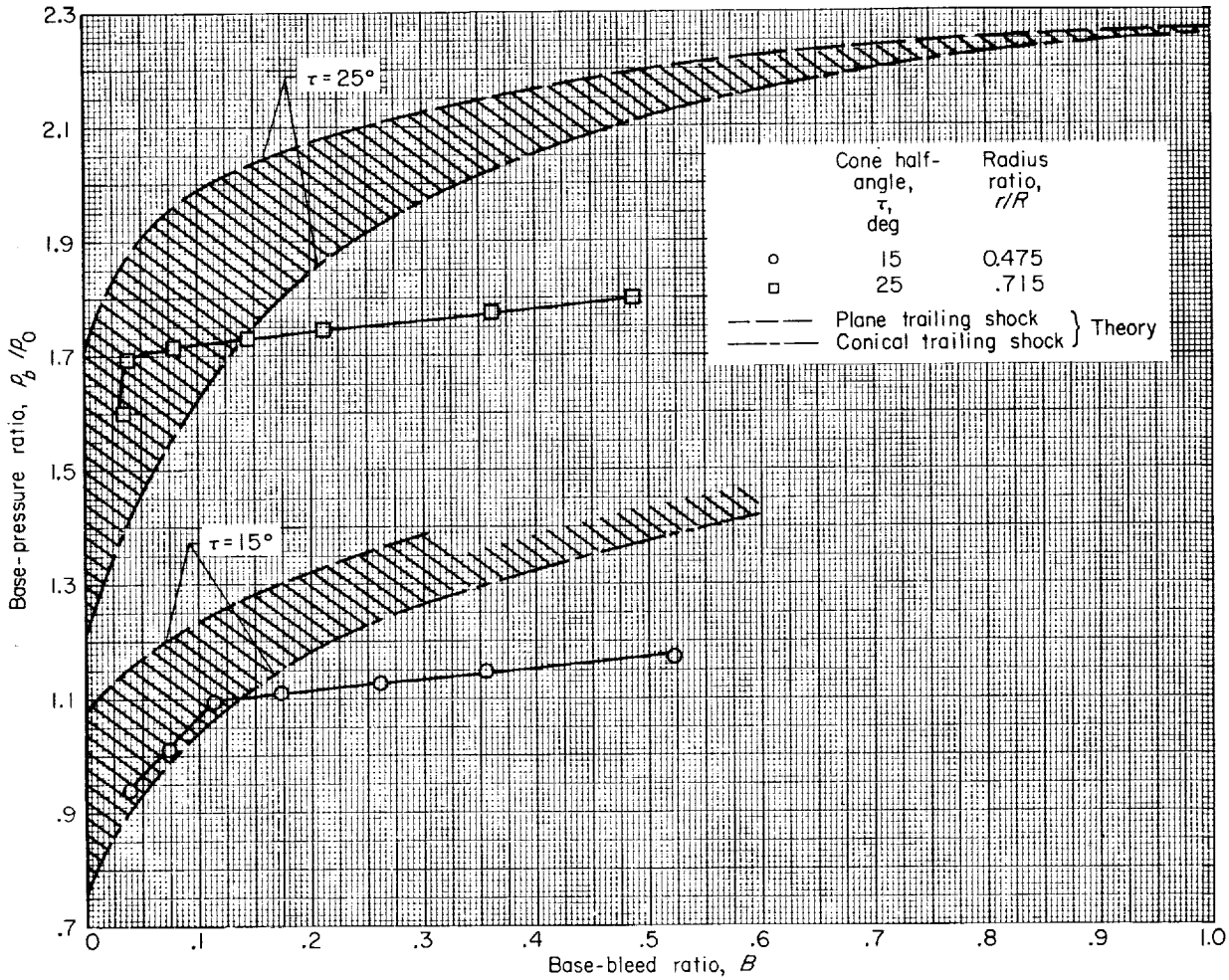

FIGURE 15.—Effect of base bleed on base pressure with conical test bodies. Mach number, 1.98.

APPENDIX A

SYMBOLS

A area

B base-bleed ratio, equal to ratio of bleed-flow rate to flow rate of free-stream air through base area of step

C Crocco number, $u/\sqrt{2c_pT}$

c_p specific heat at constant pressure

d diameter of basic body

h height of two-dimensional step

I_1 $\displaystyle\int_{-\infty}^{\eta} \frac{\varphi\, d\eta}{1-C^2\varphi^2}$ (tabulated in ref. 8)

k $\sqrt{u/\nu}$

l length of basic body from nose to base

M Mach number

m mass-flow rate

P total pressure

p static pressure

R radius of basic body

R_o gas constant

Re Reynolds number

r radius of test body at base of basic body

s distance along free streamline from step edge to intersection of free streamline and surface downstream of step

T total temperature

t static temperature

U velocity external to mixing zone

u local velocity within mixing zone

x horizontal distance from base of basic body

y radial distance from surface of basic body

α angular location on surface of test body measured from top, deg

γ ratio of specific heats

δ boundary-layer thickness

η position parameter ($\sigma y/x$ in refs. 1, 4, and 8; $y\sqrt{U_\infty/\nu_\infty x}$ in ref. 5)

θ angularity of flow direction with respect to horizontal, deg

ν kinematic viscosity

σ similarity parameter of refs. 1, 4, and 8

τ angularity of test-body surface with respect to horizontal, deg

φ velocity ratio (u/u_0 in refs. 1, 4, and 8; u/U in ref. 5)

Subscripts:

a outside of mixing or boundary-layer regions

b base region

j jet boundary streamline in mixing region defined as that for which mass flow external to it is equal to mass flow over basic body upstream of base

L laminar

l local conditions

s limiting streamline in mixing region defined as that for which mass flow between it and jet boundary streamline is equal to base-bleed flow

T turbulent

w conditions at surface of test body

$0,\infty$ free stream

1 upstream of step edge

2 between waves emanating from step edge and trailing shock

3 downstream of trailing shock wave

Superscript:

$*$ sonic

APPENDIX B

CALCULATION OF BASE-PRESSURE RATIO WITHOUT BASE BLEED

The steps needed for the solution of base-pressure ratio for a given model geometry were as follows:

(1) The flow in region 1 (see fig. 1) was assumed to be uniform with zero flow angularity and with the Mach number external to the boundary layer.

(2) The base-pressure ratio was determined by trial and error. Therefore, a value of p_b/p_0 was assumed.

(3) For axisymmetric configurations the nonmixing flow properties along the free streamline in region 2 are presented in reference 5. These results were used to determine the flow properties at the intersection of the free streamline and the test-body surface. (In many cases it was necessary to extrapolate the curves of ref. 5 to higher values of x/d to obtain the desired information.) The Mach number $M_{2,a}$ external to the mixing zone and the flow direction θ_2 of all the flow in region 2 approaching the trailing shock were assumed to be uniformly equal to those of the free streamline at the intersection. For two-dimensional configurations the flow properties in region 2 were obtained from a simple Prandtl-Meyer expansion to the assumed base pressure.

(4) The axisymmetric solution was continued from this point for two different cases: In one case the trailing shock was assumed to be a plane wave that occurred at the approach Mach number $M_{2,a}$ and produced a flow deflection $\Delta\theta=\theta_3-\theta_2$, where θ_3 was the angle of the test-body surface. In the other case the trailing shock was assumed to be a conical wave that occurred also at the approach Mach number $M_{2,a}$ and the half-angle of the hypothetical cone that produced this shock wave was $\Delta\theta=\theta_3-\theta_2$. The pressure rise p_3/p_2 of the trailing shock was then determined for each case. For the plane shock this calculation was straightforward, and for the conical shock p_3 was assumed to correspond to the cone surface pressure. The two-dimensional calculation was similar with the exception that the trailing shock was known to be a plane wave.

(5) The next step was to determine the velocity ratio φ of the limiting streamline resulting from the mixing process. Since base bleed is not considered here, this velocity ratio would be equal to that of the jet boundary streamline φ_j. This parameter is presented in reference 8 for turbulent mixing and in reference 5 for laminar mixing. (In the nomenclature of ref. 5, $\varphi_j=u/U$ evaluated at $(y/\sqrt{x})\sqrt{U_\infty/\nu_\infty}=0$.)

(6) The limiting streamline was assumed to stagnate isentropically at the test-body surface, producing a pressure rise $(P/p)_j$ that depended upon the Mach number along this streamline. This pressure rise was determined as follows:

(a) Compute $C_j=\varphi_j C_{2,a}$ knowing $M^2=\dfrac{2}{\gamma-1}\dfrac{C^2}{1-C^2}$

(b) Compute $\left(\dfrac{P}{p}\right)_j=\left(1+\dfrac{\gamma-1}{2}M_j^2\right)^{\frac{\gamma}{\gamma-1}}$

(7) If the correct p_b/p_0 was assumed in step (2), then $(P/p)_j$ from step (6)(b) would be equal to the pressure rise p_3/p_2 of step (4). If not, a different value for p_b/p_0 was assumed, and the calculation was repeated until equality was obtained. Because two different types of trailing-shock waves were assumed for axisymmetric configurations (a plane and a conical wave), there would be two different values of p_3/p_2 and hence of p_b/p_0 also. These two values of base-pressure ratio then served as a prediction of the range within which the data would be expected to be located.

APPENDIX C

CALCULATION OF PRESSURE DISTRIBUTION IN REGION OF TRAILING SHOCK

The solution of pressure distribution for a given model geometry required the following steps:

(1) The flow properties in region 1 were assumed uniform as in step (1) of appendix B.

(2) The calculation was made for a given value of base-pressure ratio. In the present analysis the experimental value was chosen rather than the theoretical value.

(3) The flow properties in region 2 were determined in the same manner as in step (3) of appendix B.

(4) Assumptions regarding the nature of the trailing shock and the calculation of its pressure rise p_3/p_2 were identical to those of step (4) of appendix B.

(5) The next step was to superimpose upon the flow in region 2 the fully developed isoenergetic mixing-velocity profiles of reference 8 for turbulent mixing and of reference 5 for laminar mixing. It was assumed that the jet boundary streamline of the mixing profile coincided in position and direction with the free streamline as determined in step (3).

(6) It was assumed that the pressure-rise distribution resulted from the isentropic stagnation of the streamlines in the mixing zone at their intersection with the surface downstream of the step. It was further assumed that this pressure-rise curve terminated upon reaching the trailing-shock pressure rise p_3/p_2 of step (4). The steps needed to accomplish this portion of the solution were as follows:

(a) The velocity ratio φ was determined as a function of the position parameter η for turbulent mixing from reference 8 and for laminar mixing from reference 5.

(b) For a given φ the corresponding M was determined from the relations $C=\varphi_1 C_{2,a}$ and $M^2=\frac{2}{\gamma-1}\frac{C^2}{1-C^2}$.

(c) Then the corresponding P/p was determined using $\frac{P}{p}=\left(1+\frac{\gamma-1}{2}M^2\right)^{\frac{\gamma}{\gamma-1}}$. Hence, the pressure ratio $p_w/p_b=P/p$ was known as a function of η.

(d) The position on the surface downstream of the step that corresponded to any given value of η was then determined. Knowing this relation, the pressure ratio corresponding to any position on the surface was known. The following relations between η and surface position can be derived from geometrical considerations. For two-dimensional configurations with turbulent mixing,

$$\frac{x}{h}=\frac{\cos\theta_3\cos\theta_2}{\sin(\theta_3-\theta_2)}-\frac{\dfrac{\eta_j-\eta}{\sigma}\cos^2\theta_3}{\sin^2(\theta_3-\theta_2)\left[1+\dfrac{\dfrac{\eta_j-\eta}{\sigma}}{\tan(\theta_3-\theta_2)}\right]}$$

For two-dimensional configurations with laminar mixing,

$$\frac{x}{h}=\frac{\cos\theta_3\cos\theta_2}{\sin(\theta_3-\theta_2)}+\frac{\left(\dfrac{\eta_j-\eta}{k_{2,a}}\right)\cos\theta_3}{\sqrt{h}\sin(\theta_3-\theta_2)}\left\{\frac{\dfrac{\eta_j-\eta}{k_{2,a}}}{\sqrt{h}\tan(\theta_3-\theta_2)}+\sqrt{\left[\frac{\dfrac{\eta_j-\eta}{k_{2,a}}}{\sqrt{h}\tan(\theta_3-\theta_2)}\right]^2+\frac{4\cos\theta_3}{\sin(\theta_3-\theta_2)}}\right\}$$

For axisymmetric configurations with turbulent mixing,

$$\frac{x}{d}\simeq\left(\frac{x}{d}\right)_w-\left(\frac{s}{d}\right)\frac{\dfrac{\eta_j-\eta}{\sigma}\cos\theta_3}{\sin(\theta_3-\theta_2)\left[1+\dfrac{\dfrac{\eta_j-\eta}{\sigma}}{\tan(\theta_3-\theta_2)}\right]}$$

where $(x/d)_w$ was the axial-distance ratio from the base to the intersection of the free streamline and the test-body surface. In all equations the algebraic sign of θ_2 was positive for $p_b/p_0>1$ and negative for $p_b/p_0<1$.

APPENDIX D

CALCULATION OF BASE-PRESSURE RATIO OF AXISYMMETRIC CONFIGURATIONS WITH BASE BLEED

For a given model geometry and base-bleed flow rate, the base-pressure ratio was calculated by the following steps:

(1) The bleed air was assumed to be at the same total temperature as the free-stream air and to enter the base region with negligible axial momentum. The base-bleed flow ratio was calculated from (for derivation see ref. 1)

$$B=\frac{m_b\sqrt{T_0}}{A_b P_0}\sqrt{\frac{R_a}{\gamma}}$$

(2) As in appendix B, a trial-and-error solution for base-pressure ratio was required. Therefore, a value for the ratio was assumed.

(3) The flow properties in region 2 were determined in the same manner as in step (3) of appendix B.

(4) Assumptions regarding the nature of the trailing shock and the calculation of its pressure rise p_3/p_2 were identical to those of step (4) in appendix B.

(5) The equation for base-bleed ratio, which for turbulent mixing can be written as

$$B=\left(\frac{2}{\gamma+1}\right)^{\frac{\gamma+1}{2(\gamma-1)}}\frac{[I_1(C_{2,a};\eta_j)-I_1(C_{2,a};\eta_s)]}{\sigma\left(\frac{T}{t}\right)_{M_{2,a}}\left(\frac{A}{A^*}\right)_{M_{2,a}}}\frac{s/d}{A_b/d}$$

was solved for $I_1(C_{2,a};\eta_s)$, where $(T/t)_{M_{2,a}}$ and $(A/A^*)_{M_{2,a}}$ are the isentropic flow parameters evaluated at $M_{2,a}$; A_b is the base area in the plane of the base; and I_1 is an integral of flow properties in the mixing zone that is tabulated in reference 8 as a function of η. From these tables the value of $I_1(C_{2,a};\eta_j)$ to be used in the preceding equation was found, as was the position parameter of the limiting streamline η_s, corresponding to the calculated value of $I_1(C_{2,a};\eta_s)$.

(6) The remaining calculations were:

(a) Determine the φ_s that corresponded to η_s from reference 8.

(b) Compute $C_s=\varphi_s C_{2,a}$.

(c) Compute $\left(\frac{P}{p}\right)_s=\left(1+\frac{\gamma-1}{2}M_s^2\right)^{\frac{\gamma}{\gamma-1}}$. If $(P/p)_s$ was not equal to p_3/p_2 of step (4), a different value of p_b/p_0 was assumed in step (2), and the calculation was repeated until equality was obtained. The two values of p_b/p_0 thus obtained (one corresponding to a plane and the other to a conical trailing shock) then served to predict a range for the experimental data.

REFERENCES

1. Korst, H. H., Page, R. H., and Childs, M. E.: A Theory for Base Pressures in Transonic and Supersonic Flow. Tech. Note 392–2, Eng. Exp. Station, Univ. Ill., Mar. 1955. (Contract AF–18(600)–392.)
2. Chapman, Dean R., Kuehn, Donald M., and Larson, Howard K.: Investigation of Separated Flows in Supersonic and Subsonic Streams with Emphasis on the Effect of Transition. NACA Rep. 1356, 1958. (Supersedes NACA TN 3869.)
3. Chapman, Dean R.: An Analysis of Base Pressure at Supersonic Velocities and Comparison with Experiment. NACA Rep. 1051, 1951. (Supersedes NACA TN 2137.)
4. Korst, H. H., Page, R. H., and Childs, M. E.: Compressible Two-Dimensional Jet Mixing at Constant Pressure. Tech. Note 392–1, Eng. Exp. Station, Univ. Ill., April, 1954. (Contract AF–18(600) 392.)
5. Chapman, Dean R.: Laminar Mixing of a Compressible Fluid. NACA Rep. 958, 1950. (Supersedes NACA TN 1800.)
6. Murthy, K. R. Ananda, and Hammitt, A. G.: Investigation of the Interaction of a Turbulent Boundary Layer with Prandtl-Meyer Expansion Fans at $M=1.88$. Rep. 434, Princeton Univ., Aug. 1958.
7. Sims, Joseph L.: Results of the Computations of Supersonic Flow Fields Aft of Circular Cylindrical Bodies of Revolution by the Method of Characteristics. Rep. DA–R–49, Dev. Operations Div., Army Ballistic Missile Agency, Mar. 1958.
8. Korst, H. H., Page, R. H., and Childs, M. E.: Compressible Two-Dimensional Jet Mixing at Constant Pressure. Tables of Auxiliary Functions for Fully Developed Mixing Profiles. Tech. Note 392–3, Eng. Exp. Station, Univ. Ill., Apr. 1955. (Contract AF–18(600)–392.)
9. Schlichting, H.: Lecture Series "Boundary Layer Theory." Pt. I—Laminar Flows. NACA TM 1217, 1949.
10. Schlichting, H.: Lecture Series "Boundary Layer Theory." Pt. II—Turbulent Flows. NACA TM 1218, 1949.
11. Chiccine, Bruce G., Valerino, Alfred S., and Shinn, Arthur M.: Experimental Investigation of Base Heating and Rocket Hinge Moments for a Simulated Missile Through a Mach Number Range of 0.8 to 2.0. NASA TM X–82, 1959.
12. Sivier, Kenneth R., and Bogdonoff, Seymour M.: The Effect of Support Interference on the Base Pressure of a Body of Revolution at High Reynolds Numbers. Rep. 332, Princeton Univ., Oct. 1955.
13. Wu, Chen Yuan: The Influence of Finite Bleed Velocities on the Effectiveness of Base Bleed in the Two-Dimensional Supersonic Base Pressure Problem. Ph.D. Thesis, Univ. Ill., 1957.
14. Chow, W. L.: On the Base Pressure Resulting from the Interaction of a Supersonic External Stream with a Sonic or Subsonic Jet. Jour. Aero/Space Sci., vol. 26, no. 3, Mar. 1959, pp. 176–180.
15. Fuller, L., and Reid, J.: Experiments on Two-Dimensional Base Flow at $M=2.4$. R. & M. 3064, British RAE, 1958.
16. Beastall, D., and Eggink, H.: Some Experiments on Breakaway in Supersonic Flow, pt. II. Tech. Note AERO 2061, British RAE, June 1950.

U.S. GOVERNMENT PRINTING OFFICE: 1961